Table, Figure 및 결과 다듬기

성균관대학교 의과대학 삼성서울병원 내과 이준행

결과 작성을 위한 checklist

- 기본적인 연구 결과들을 제공하였는가?
- 주요 발견의 효과 크기는 찾아보기 쉬운가?
- 본문의 표와 그림을 보완하고 있는가?
- 표본수에 비하여 기술적 결과와 분석적 결과의 정밀도는 합당한가?
- 특이한 또는 놀라운 발견에 대한 내용은 적절한 곳에 위치하고 있는가?

우리의 목표: 쉽고 정보가 많은 표

Table 3—*Demographic Characteristics of GERD-Positive and GERD-Negative Patients With the Nodular Bronchiectatic Form of NTM Lung Disease**

Characteristics	GERD Positive (n = 15)	GERD Negative (n = 43)	p Value
Age, yr	56 (43–63.5)	57 (53–66.5)	0.320
Female gender	13 (87)	37 (86)	1.000
Body mass index, kg/m^2	20.0 (18.6–21.7)	20.6 (19.5–22.2)	0.316
Smoking status			
Non-smoker	14 (93)	40 (93)	1.000
Ex-smoker	1 (7)	3 (7)	
Etiology			
M avium complex	5 (33)	22 (51)	0.368
M abscessus	10 (67)	21 (49)	
AFB smear positive	12 (80)	19 (44)	0.033
Involved lobes on HRCT, No.			
Bronchiectasis	4 (3–4)	2 (2–3)	0.008
Bronchiolitis	4 (3–5)	2 (2–4)	0.005
Pulmonary function tests			
FVC, % of predicted	93.0 (83.0–102.0)	87.0 (77.5–93.5)	0.170
FEV_1, % of predicted	92.5 (76.5–107.0)	88.0 (72.5–102.0)	0.508
FEV_1/FVC, ratio	76.0 (67.0–84.0)	74.0 (71.0–80.0)	0.880
Peak expiratory flow, % of predicted	92.0 (80.0–111.5)	96.0 (74.5–99.0)	0.748

*Data are presented as the median (interquartile range) or No. (%). Bronchiolitis was defined as the presence of small centrilobular nodules (< 10 mm in diameter) or branching nodular structures (tree-in-bud pattern) on HRCT.

표 점검표

- 제목이 장황하지 않고도 충분히 서술적인가?
- 줄과 칸이 깔끔한가?
- 불필요한 자료, 반복되는 연구대상자 수 표시, 지나친 정밀함, 의미가 모호한 약자들이 있지는 않는가? **꼭 이렇게 자세할 필요가 있는가?**
- 본문을 보지 않고도 모든 항목의 의미를 명확히 알 수 있는가?
- 두 개 이상의 표를 하나로 묶을 수 없는가?
- 모든 표를 본문에서 언급하였나? 또한 순서대로 언급하였나?

Browner. Publishing and presenting clinical research (번역본 91쪽)

좋지 못한 제목의 예와 개선안

좋지 못한 제목	개선된 제목
Characteristics of subjects	Characteristics of the 54 men enrolled in the trial
Comparison of active treatment with diuretic therapy compared with placebo in 122 men	Effects of treatment of hypertension and placebo groups
Predictors of quality of life	Factors associated with differences in quality of life: multivariate models
Independent ($p<0.05$) predictors of quality of life using logistic regression following stepwise selection procedures, using the criteria of reference 6	↑

Browner. Publishing and presenting clinical research (번역본 90쪽)

우리의 목표: 쉽고 기억하기 쉬운 그림

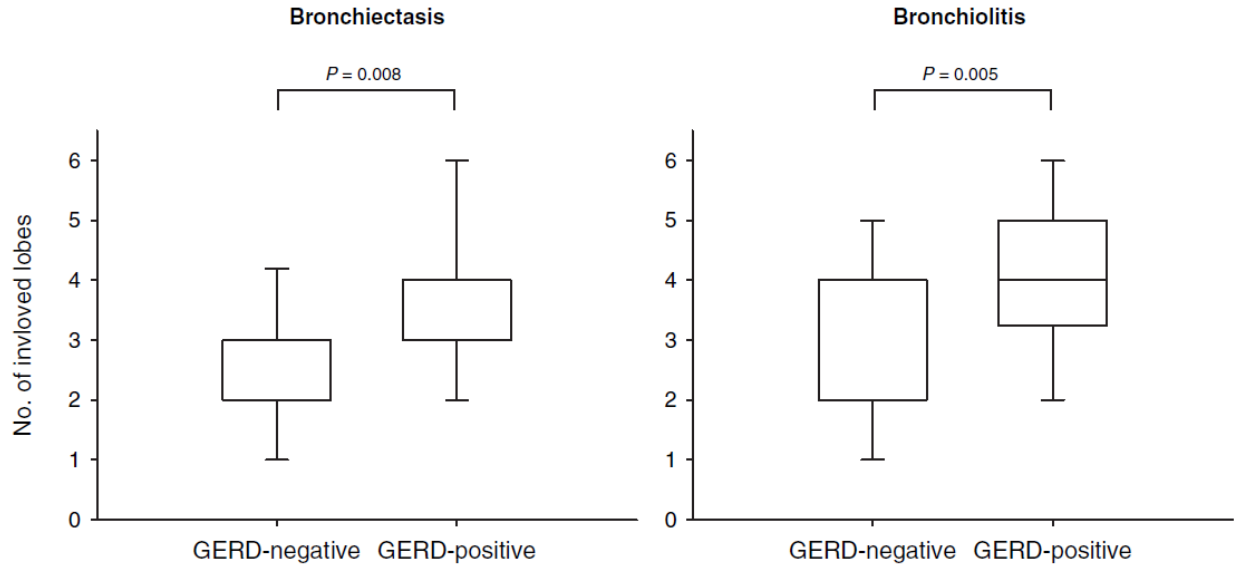

FIGURE 1. Box-and-whiskers graph of the quantitative imaging analysis showing the number of involved lobes with bronchiectasis and bronchiolitis. Bronchiolitis is defined as the presence of centrilobular small nodules (< 10 mm in diameter) or branching nodular structures (tree-in-bud pattern) on HRCT. The ends of the boxes indicate the 25th and 75th percentiles, and the lines in the bars indicate the median value. The 10th and 90th percentiles are indicated with whiskers. In the patients without GERD, the median numbers of involved lobes with bronchiectasis and bronchiolitis are both 2. In the patients with GERD, the median numbers of involved lobes with bronchiectasis and bronchilitis are both 4. Bronchiectasis and bronchiolitis were observed in more lobes in pateints with GERD than in patients without GERD ($p = 0.008$ and $p = 0.009$, respectively).

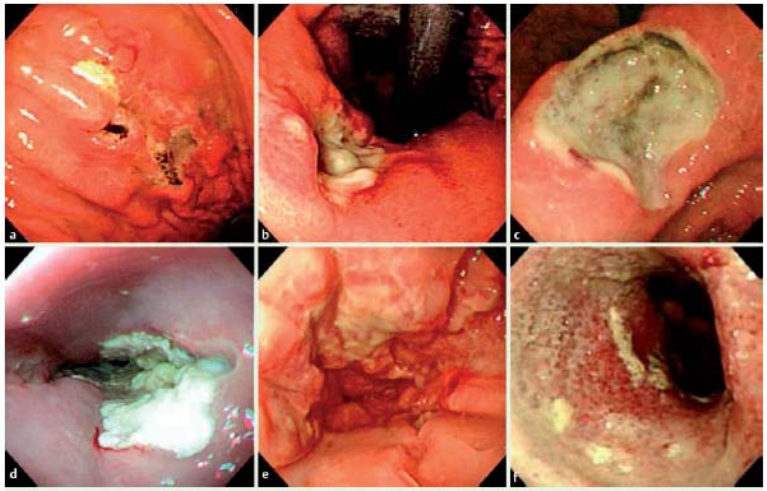

Figure 1 Endoscopic appearances of primary upper gastrointestinal NK-/T-cell lymphoma. a Superficial/erosive type (patient 1): several superficial erosions of various sizes in a continuous focal pattern in the body of the stomach. b Ulcerative type (patient 2): a round 1.5-cm well defined deep ulcer in the body of the stomach. c Ulcerative type (patient 3): round 2-cm well defined deep ulcer at the angle of the stomach. d Ulcerative type (patient 4): a long irregular 4-cm well defined deep ulcer in the mid esophagus. e Ulceroinfiltrative type (patient 5): diffuse ill defined ulcers of various sizes in a continuous pattern in the lower esophagus. f Ulceroinfiltrative type (patient 6): diffuse ill defined ulcers of various sizes in a continuous pattern in the second portion of the duodenum.

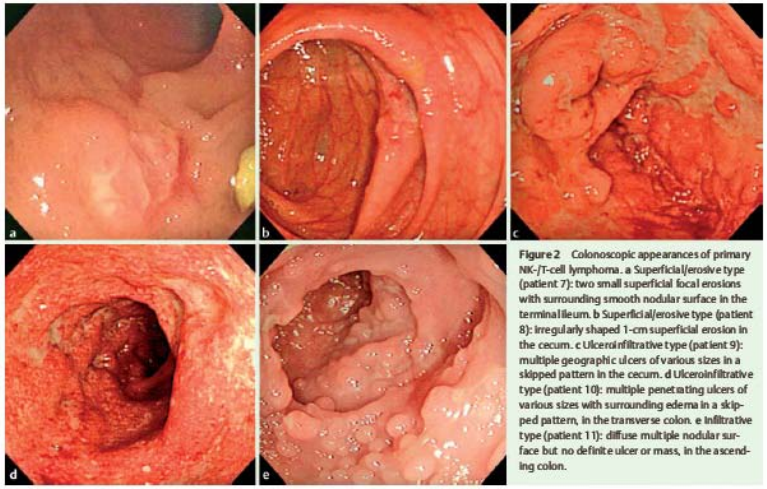

Figure 2 Colonoscopic appearances of primary NK-/T-cell lymphoma. a Superficial/erosive type (patient 7): two small superficial focal erosions with surrounding smooth nodular surface in the terminal ileum. b Superficial/erosive type (patient 8): irregularly shaped 1-cm superficial erosion in the cecum. c Ulceroinfiltrative type (patient 9): multiple geographic ulcers of various sizes in a skipped pattern in the cecum. d Ulceroinfiltrative type (patient 10): multiple penetrating ulcers of various sizes with surrounding edema in a skipped pattern, in the transverse colon. e Infiltrative type (patient 11): diffuse multiple nodular surface but no definite ulcer or mass, in the ascending colon.

그림 점검표

- 모든 그림은 요점을 명확히 표현하고 있는가?
- 축, 선, 막대 및 점에 대한 표시가 있는가? 척도는 맞는가?
- **각각의 그림에 제목을 제외한 그림 설명을 붙였는가?**
- 본문은 그림을 보완하여 설명하고 있는가?
- 모든 그림을 본문에서 언급하였나? 또한 순서대로 언급하였나?
- 개인식별이 가능한 정보가 들어가 있지 않은가?

Browner. Publishing and presenting clinical research (번역본 124쪽)

그림을 조작하는 사례가 많습니다.

Nature 2005;434:952-953

CSI: cell biology

Digital photography and image-manipulation software allow biologists to tweak their data as never before. But there's a fine line between acceptable enhancements and scientific misconduct. Helen Pearson investigates.

In a cramped office in midtown Manhattan, a forensics expert peers intently at a flickering computer screen. The shadowy image, hugely magnified, reveals a tell-tale dark smear. Something about it, she can tell, is just not right…

It could come straight from the screenplay of the latest hit TV crime show. But, in fact, such scenes are playing out regularly at the sedate headquarters of Rockefeller University Press — where the images under scrutiny are those of cells and gels in papers accepted for publication in *The Journal of Cell Biology*.

In the vast majority of cases, the perpetrators aren't willfully misrepresenting their results — rather, they are unaware that their efforts to achieve the cleanest images for publication have crossed the line of acceptability. Such ignorance is widespread, and for Rossner it underlines why his journal now subjects all accepted papers to image forensics. "My goal is to catch problems before we publish," he says.

The availability of digital cameras and image-manipulation programs such as Photoshop has made it all too easy for than they used to. And researchers, some burnt by questions about their own photos' integrity, are beginning to patrol the activities of their lab members. "We all underestimate the amount of skullduggery that goes on," says Joseph Gall, who studies the structure of cell nuclei at the Carnegie Institution in Baltimore, Maryland.

Picture perfect

Biologists have always gone to great lengths to create beautiful pictures that best illustrate their data. Geneticists carry out multiple exposures of radioactively labelled DNA fragments separated on gels in order to create a crisp image. Cell biologists once worked through rolls of film to grab the perfect shot from a microscope. But with Photoshop, a few clicks of the mouse can transform a featureless black microscope snap into a starry vista littered with labelled proteins. "You can make up almost any image you want nowadays," says Tom Misteli, a cell biologist at the National Cancer Institute in Bethesda, Maryland.

Some biologists seem to succumb to this temptation. In 1989–90, only 2.5% of allegations examined by the US Office of

그림을 조작하는 사례가 많습니다.

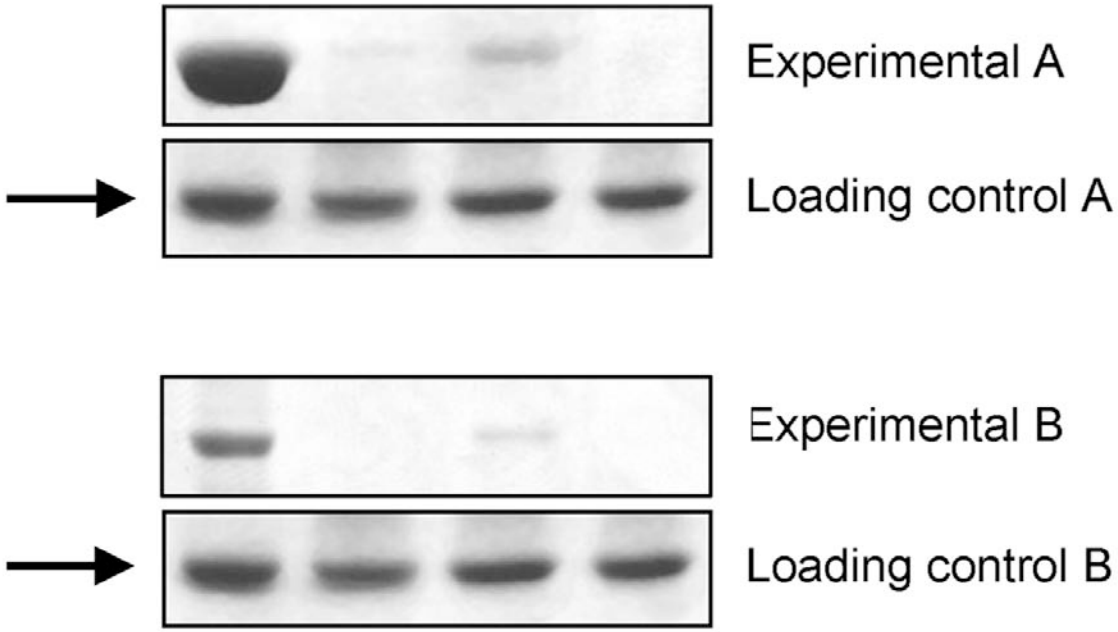

Figure 2. **Gross manipulation of blots.** Example of a duplicated panel (arrows).

J Cell Biol 2004:166:11-15

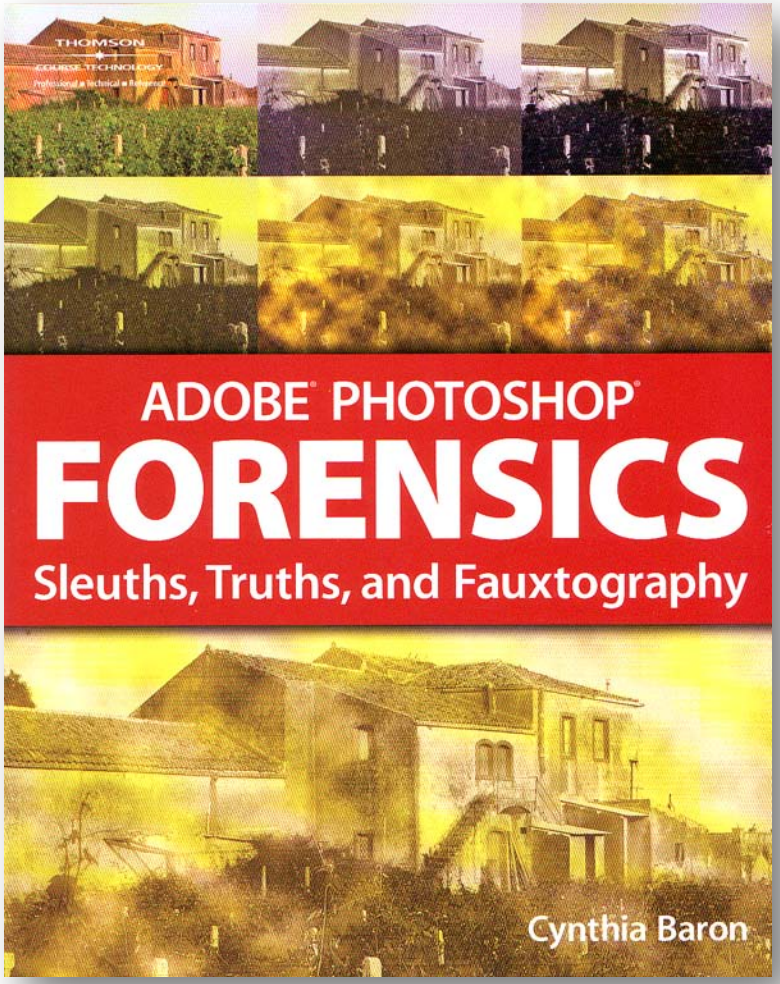
THOMSON
COURSE TECHNOLOGY
ADOBE® PHOTOSHOP®
FORENSICS
Sleuths, Truths, and Fauxtography
Cynthia Baron

Piltdown Man was a clever forgery. Instead, even as other finds around the world pointed consistently to a very different evolutionary path, people were forced to make room for Piltdown's big brain and primate jaw.

Finally, in 1953, anthropologist Joseph Weiner investigated and then documented the details of the hoax. A closer look found that the teeth of a modern ape jaw had been filed down to look like human molars. The skull had probably been dug up from a medieval grave, and all the bones had been stained to make them appear old.

Even after all this time, the forger has not definitively been named. Most people believe the finger points to Charles Dawson himself, particularly after Weiner's research found a pattern of deception in his earlier archeological digs. Yet almost every other man involved in the story has had his turn in the role, and some of them are almost as likely candidates—which doesn't speak well of the level of academic honesty a hundred years ago.

The Neverending Fraud

Outside the scientific community, we don't always realize how serious such fakery can be. But bad science contributes to the misuse of millions of dollars in government and corporate grants. It misrepresents reality to the public, creating panic or prompting bad political and social decisions. It can delay medical cures by misdirecting effort and funding to fantasyland.

And once a bad paper gets published, it lives a kind of half-life in the community. Even if the authors retract a paper (or are asked to retract it, which is much the same thing but considerably more embarrassing), the paper is still searchable online and continues to live in its original form in libraries and labs. Doctoral students looking for citations to bolster their own work may continue to cite it.

The Korean Stem Cell Scandal

The high-profile science fraud cases that do splatter the news media come to light in part because the field they're in is hot. There are dozens of other researchers competing to be the first to make a breakthrough. When someone beats them to it, they do the experiments to see if they get the same results. If they can't, they try to find out why. Ultimately, no fraud can withstand such a concentrated assault. But that process can take a long while—frequently years, like the Piltdown Man fiasco.

In other cases, a single image was divided into two, either to separate two cells on the same slide or to crop one cell into two images (Figures 6-20 and 6-21).

Figure 6-20 These two cells, which were split between the two pages in Figure 6-18, are two halves of the same cell.

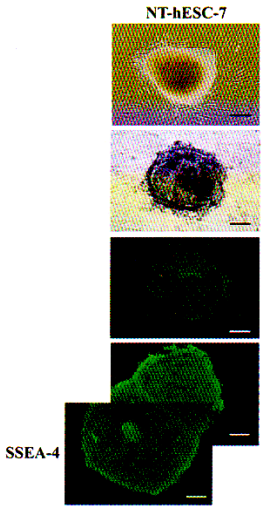

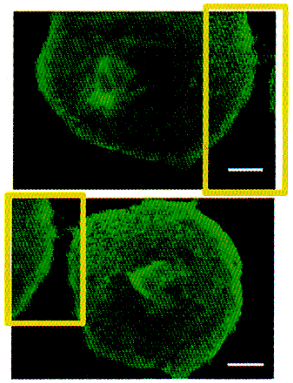

Figure 6-21 The images outlined in yellow are two views of the same two cells.

At first, Hwang claimed that some of the figures had been inserted in the paper by mistake, which was sloppy but an honest mistake. But little by little, it became clear that Hwang and his team had not successfully cloned a single human stem cell.

Having resigned in disgrace and been indicted for fraud and embezzlement in 2006, Hwang has still never admitted to any form of misconduct. He blames his team of researchers for deliberate sabotage and for creating false data on their own. As of June 2007, he was looking for new partners in other countries to continue his research.

Moving Forward

One of the outcomes of the Hwang shocker has been the increased scrutiny given to other papers involving stem cells and cloning research. All of the major scientific journals have published new guidelines on how to prepare figures and have warned that they will reject new papers that don't live up to standards.

Figure에 대한 그래픽적 접근

성균관대학교 의과대학 삼성서울병원 내과 이준행

왜 내과의사가 그래픽을 강의하나?

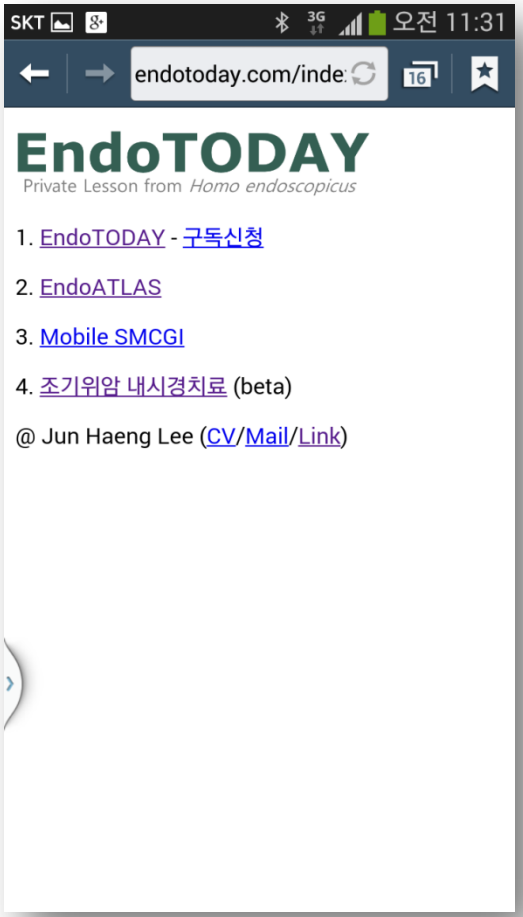

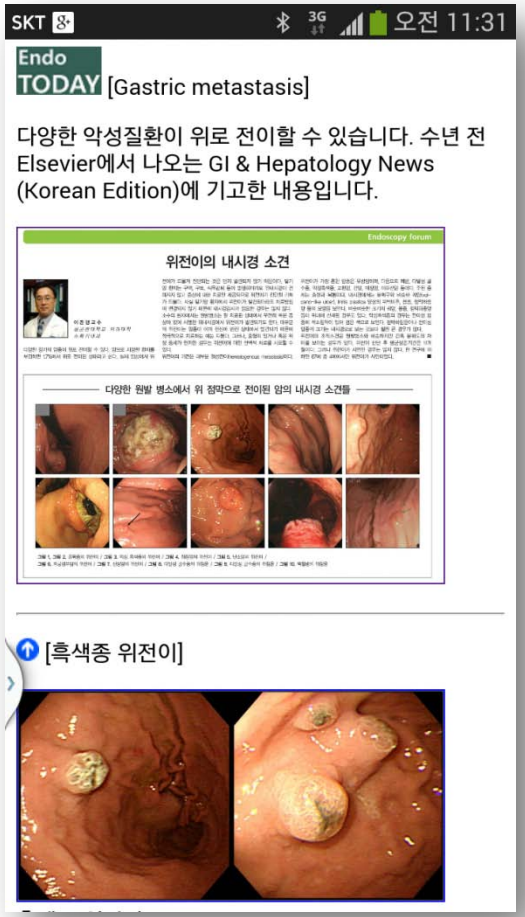

Digital mind? (Digital image mind?)

- Digital camera를 월 1회 이상 사용?
- Photoshop을 월 1회 이상 사용?
- BMP file과 JPEG file의 차이?
- Lossy / lossless compression의 차이?
- Bitmap image와 vector image의 차이?
- Powerpoint file을 만들 때 file 크기에 신경을 쓴다.

그래픽의 기본을 배우는 이유 (1/2)

- 우리는 digital native가 아니다. 자라면서 배우지 못했기 때문에 필요한 사람은 찾아서 익혀야 한다.
- 모든 발표는 PowerPoint를 이용해야 한다.
- 논문에 들어갈 그림이나 사진을 “Combination halftones, 600 dpi, TIFF without compression, CYMK”와 같은 알 수 없는 형식의 파일로 만들어 보내야 한다.

그래픽의 기본을 배우는 이유 (2/2)

- 복잡한 작업은 컴퓨터 그래픽 전문가에게 의뢰하는 것이 나을 수 있다.
- 사소한 작업까지 전문가의 도움에 기대는 것은 비효율적이다.
- 원본 자료를 허술하게 관리한 상태에서 그래픽 전문가에게 부탁한들 별 도움을 받지 못하는 예가 많다.
- **아는 것이 힘이다.**

오늘 강의가 끝난 후 여러분은...

- 논문 투고규정에 적합한 graphic image를 만들 수 있습니다.
- 적절하게 조절된 image file을 이용하여 PowerPoint file을 만들 수 있습니다.

강의 내용

- 해상도란 무엇인가?
- 비트맵 이미지와 백터 이미지
- 논문제출을 위한 적절한 해상도는?
- [Tip] PowerPoint 이미지를 TIFF로 바꾸는 방법

Topic 1

해상도란 무엇인가?

성균관대학교 의과대학 삼성서울병원 내과 이준행

논문의 그림은 4 가지 종류가 있다

- Statistical graphs, charts, and simple diagrams
- Photographic images (color photos, radiographs, ultrasound images, CT scans, MRI scans, electron micrographs, and photomicrographs)
- Illustrations
- Videos

→ 4 형태에 모두 **해상도**라는 개념이 들어가야 한다.

해상도란 무엇인가?

- 해상도(解像度)는 어느 일정한 단위 안에서 얼마나 더 자세하게 그 내용을 표현하는가를 나타내는 용어이다.
- 일정한 물리적 길이 단위인 1인치(25.4mm) 안에 표현되는 화소(pixel)의 수를 말한다. 단위로 dpi(dots per inch)가 쓰인다. 예를 들어, 72 dpi라고 하면 1인치 안에 72개의 점이 들어간다는 뜻이다.

http://ko.wikipedia.org/

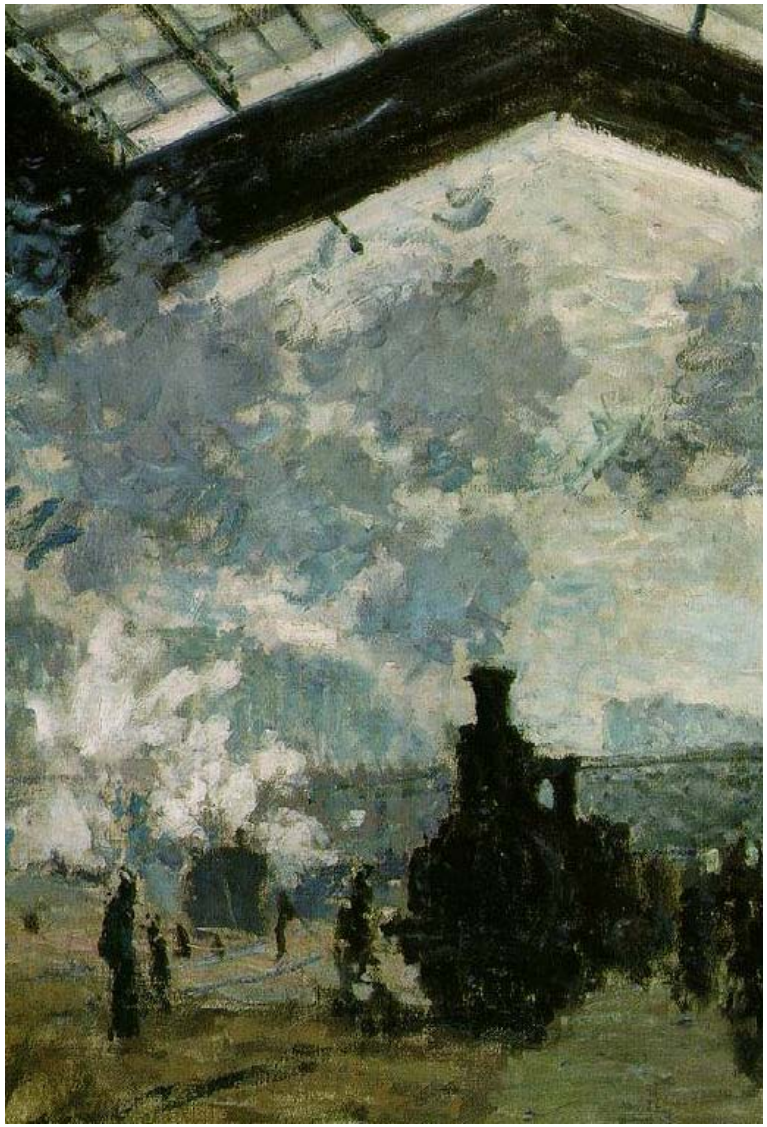

http://www.ibiblio.org/wm/paint/auth/monet/paris/

출력시 크기가 같다면 pixel의 수가 많을수록 해상도가 높다 (높은 DPI 값)

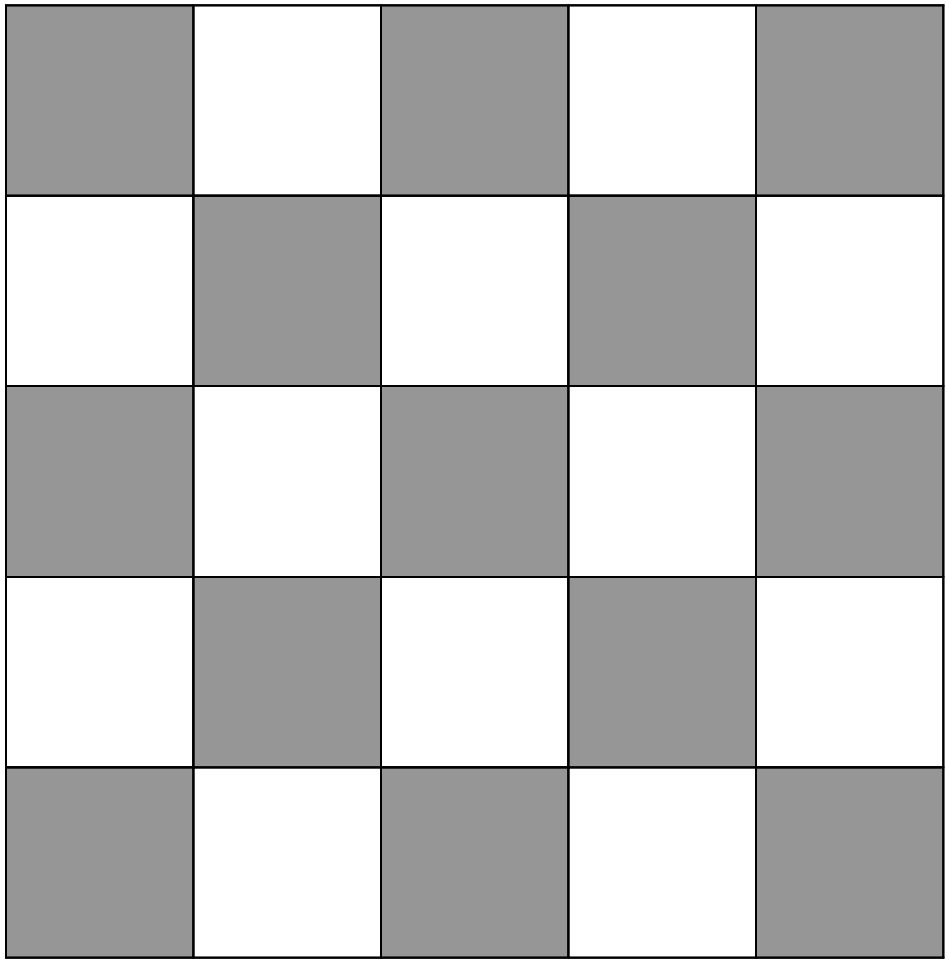

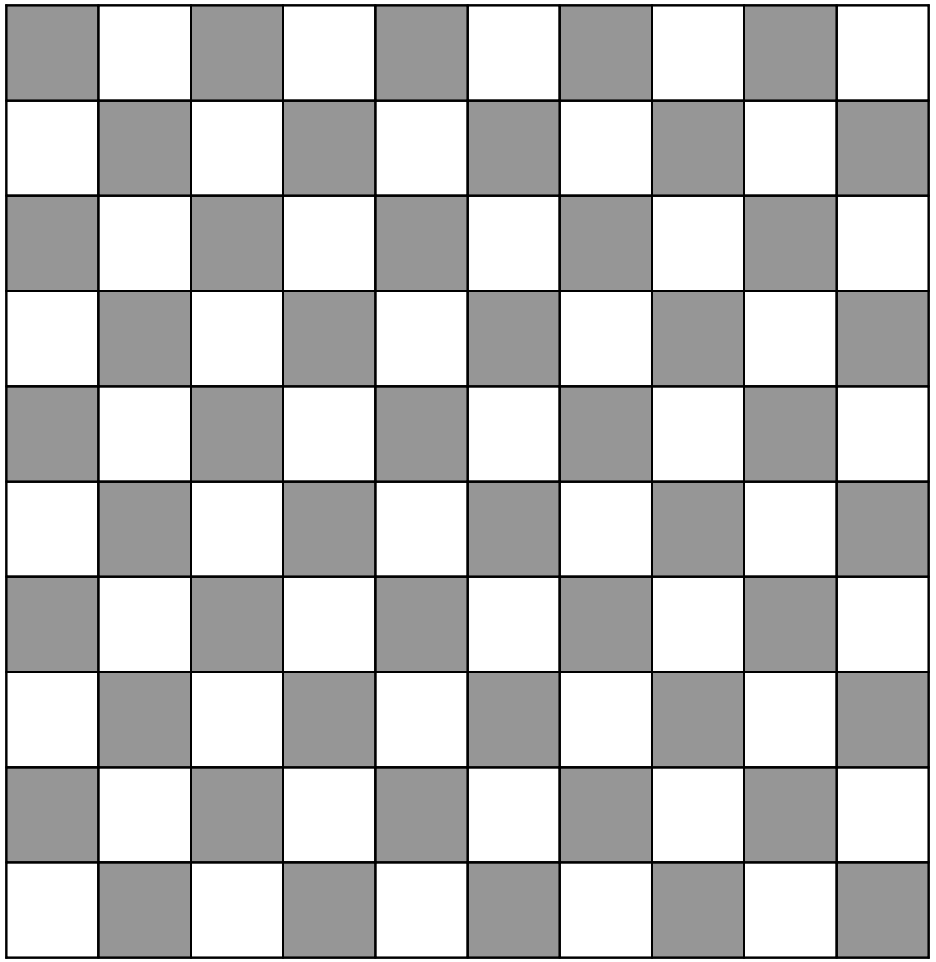

DPI = Dots / Inch

DPI value for digital image?

- A digitally stored image has ***no inherent physical dimensions***, measured in inches or centimetres.

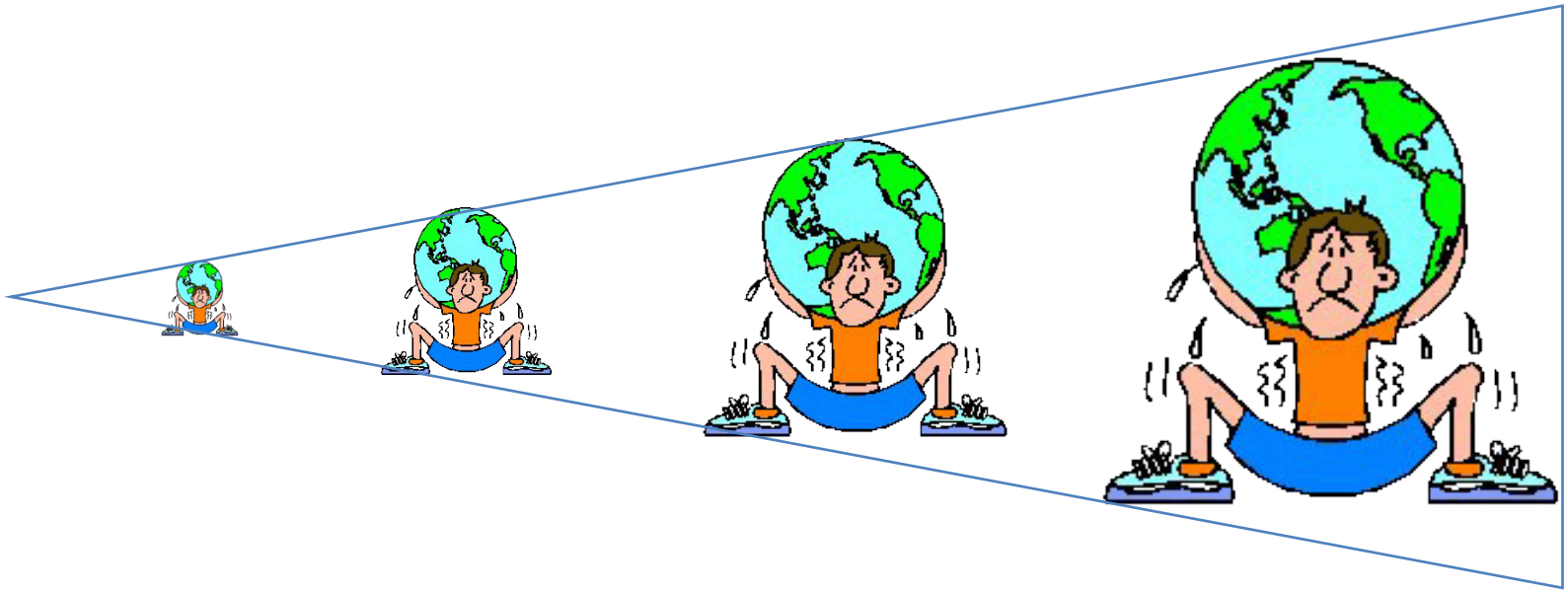

http://en.wikipedia.org/wiki/Dots_per_inch

DPI는 출력을 전제로...

- sungkyunkwan.jpg
- 85,109 byte
- 890 x 890 = 792,100 pixels
- Resolution: dots per inch (dpi)

출력을 하지 않는
한 아무런 의미가
없는 숫자이다

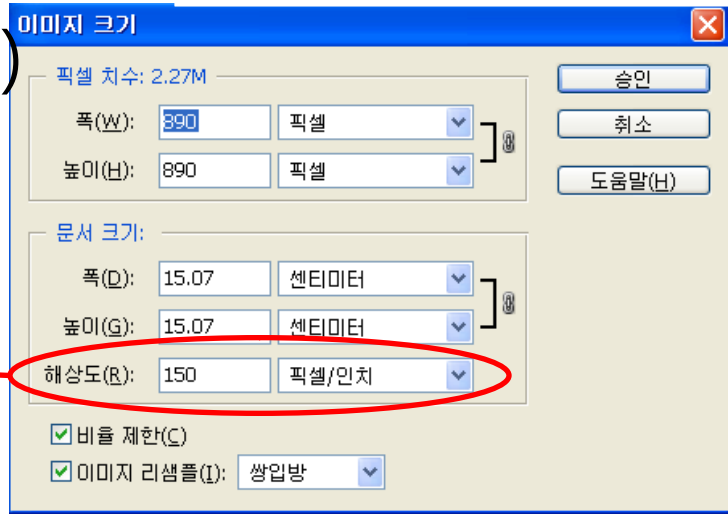

Information amount in a bitmap image

- Determined by the number of pixels
- Size (inches) x resolution (dpi) = pixel numbers

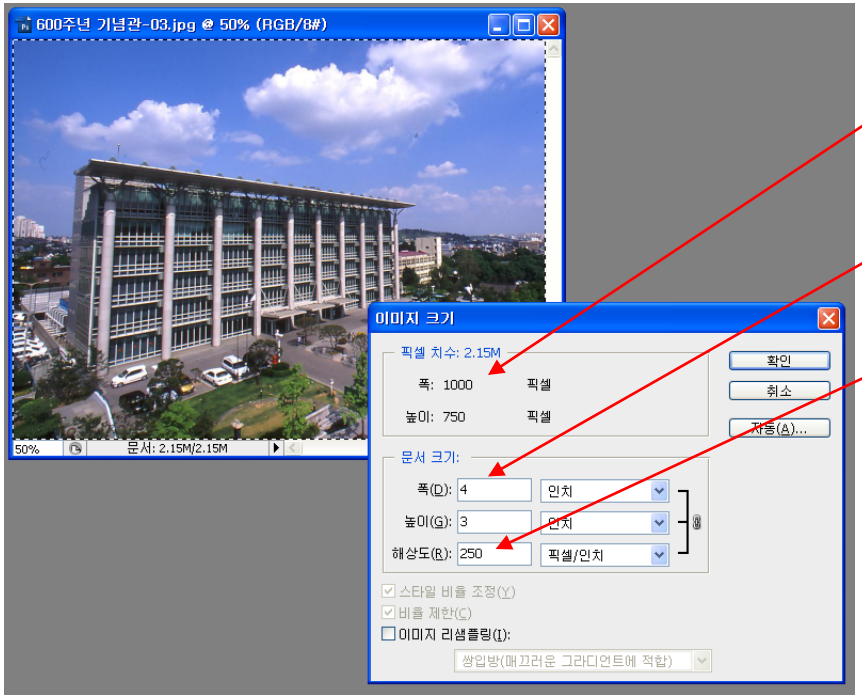

Width 1000 pixels

= 4 inches x 250 pixel/inch

Digital image에서는 pixel 수가 많을수록 정보량이 많다 (높은 해상도)

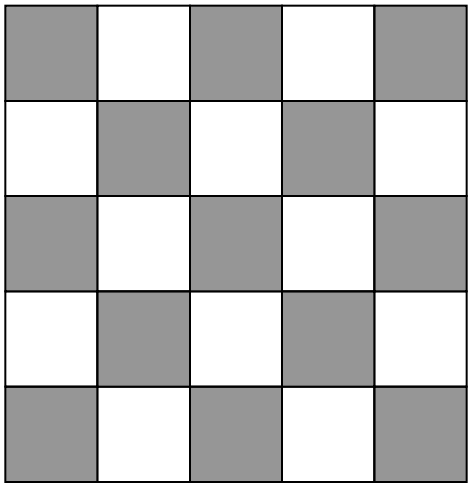

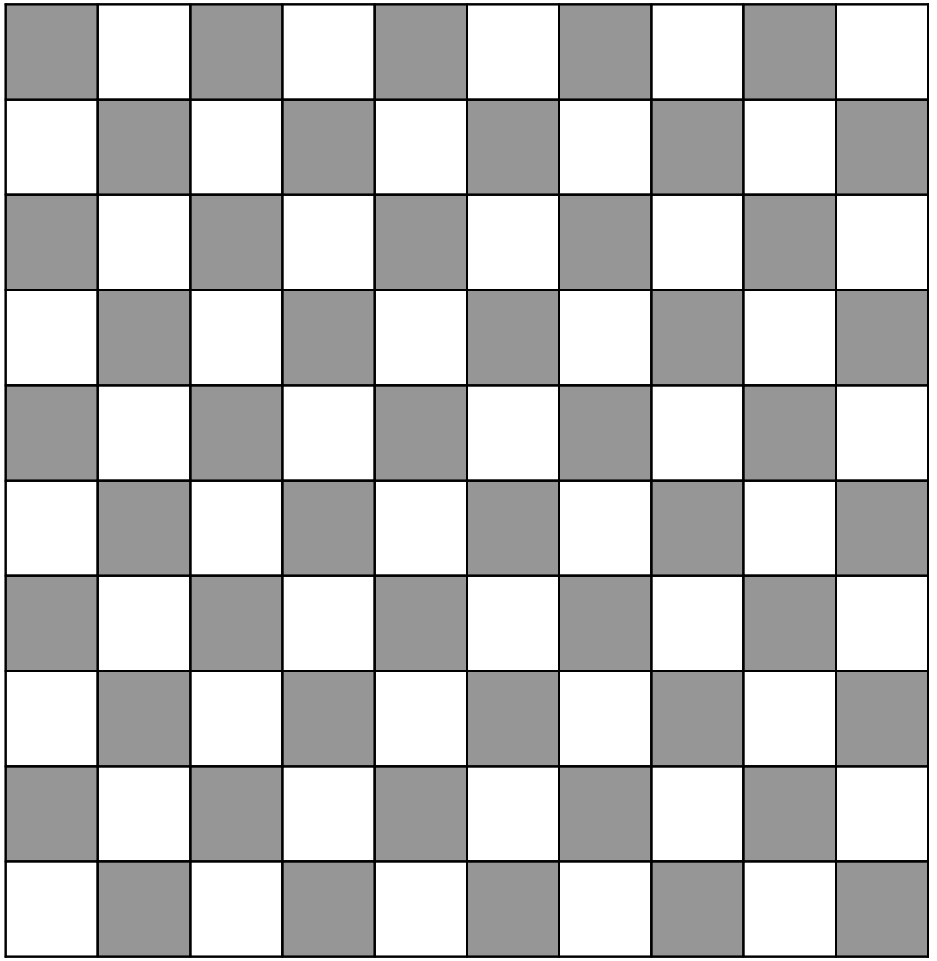

Pixel 수가 많다고 항상 고해상도는 아니다

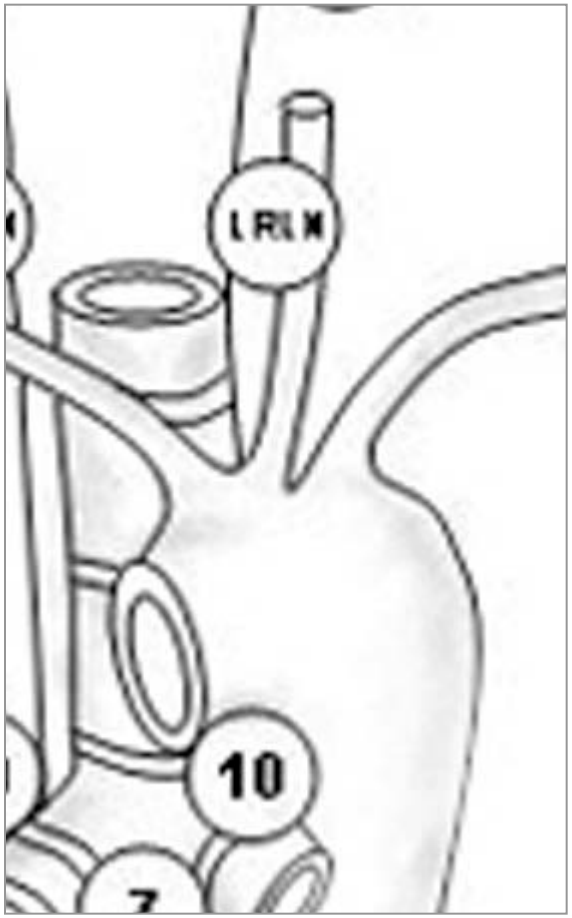

1.14 inch, 300 dpi

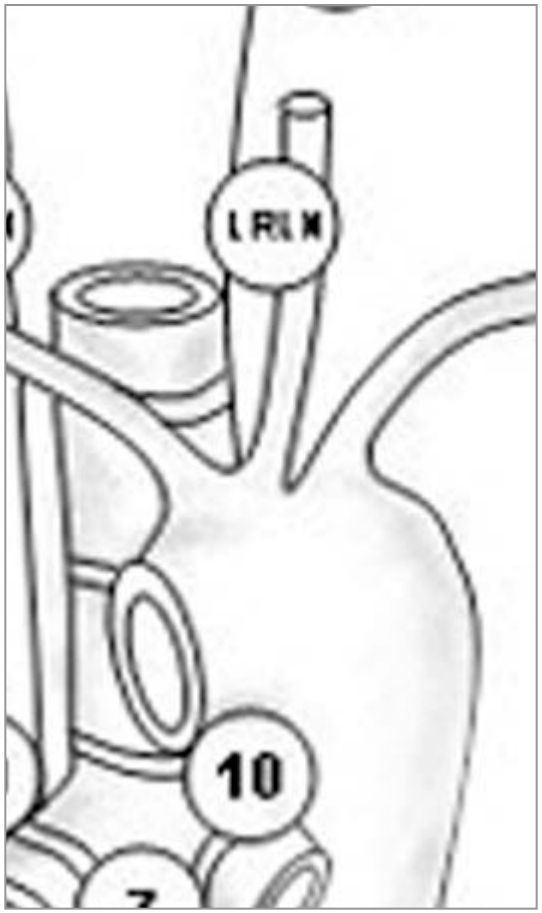

4 inch, 900 dpi

한번 줄인 pixel 수는 되돌이킬 수 없다

- 억지로 pixel 수를 늘려도 정보의 양은 늘지 않는다

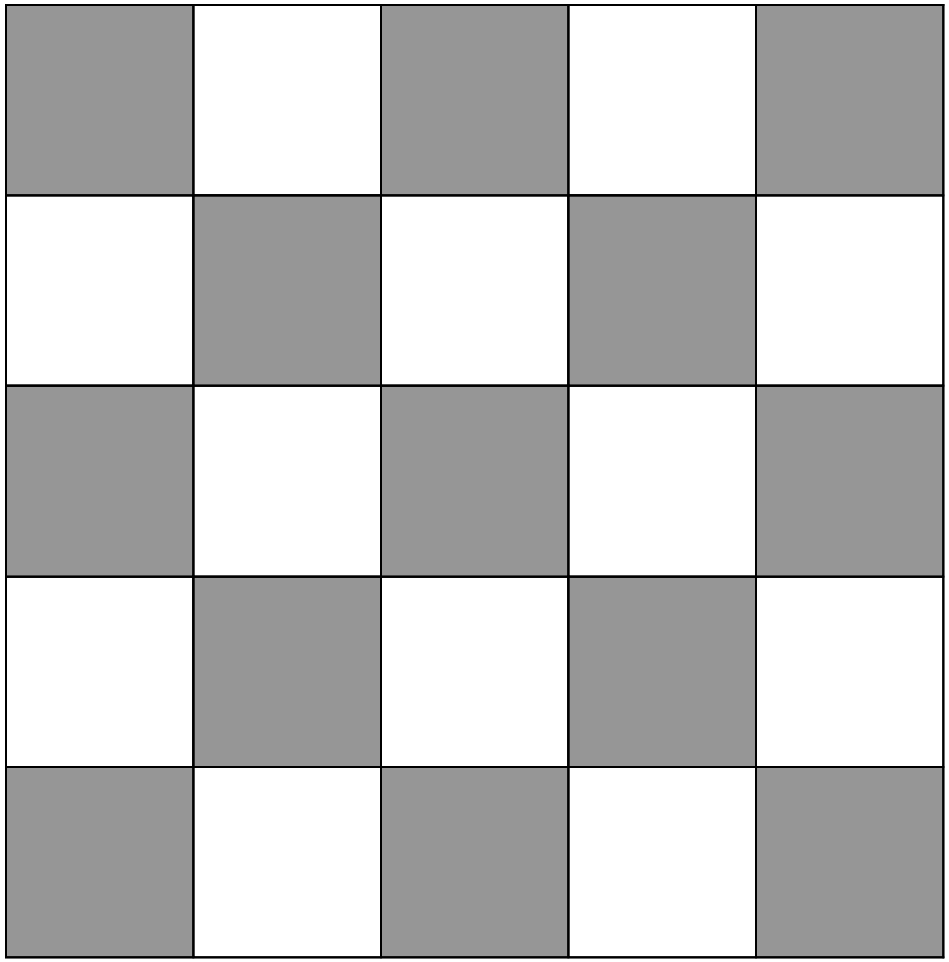

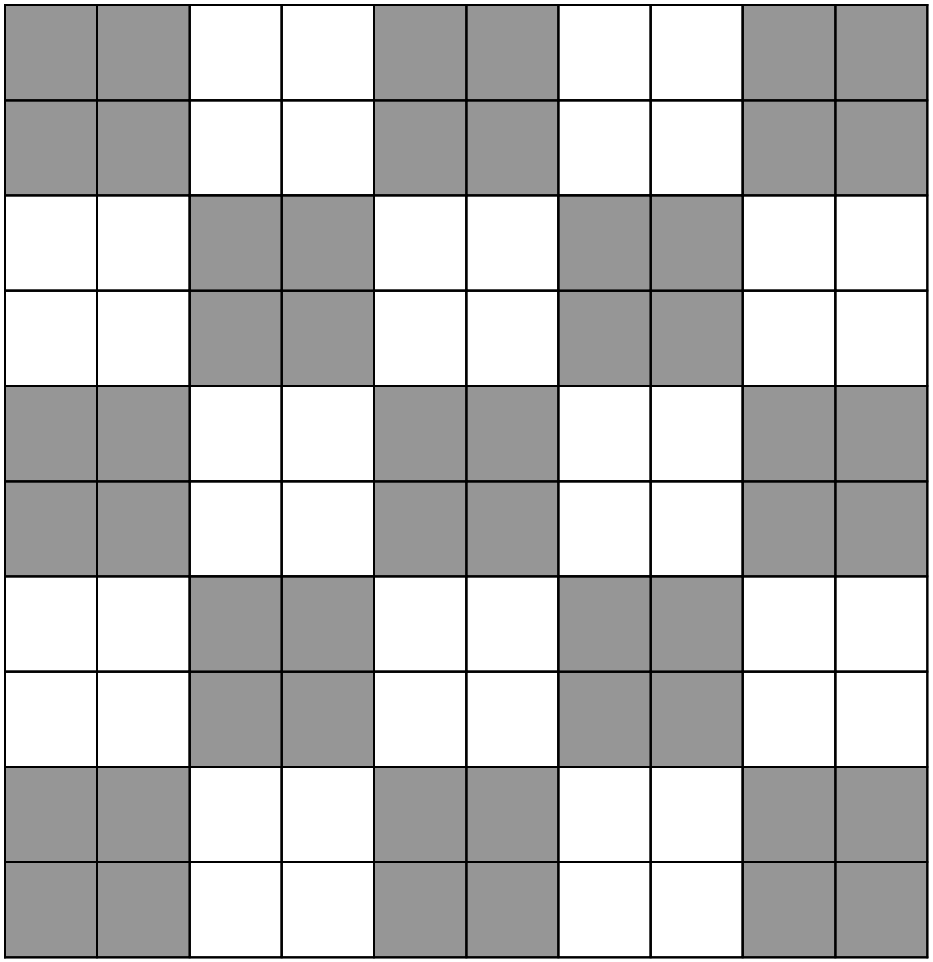

Population bottleneck

- an important concept from evolutionary biology

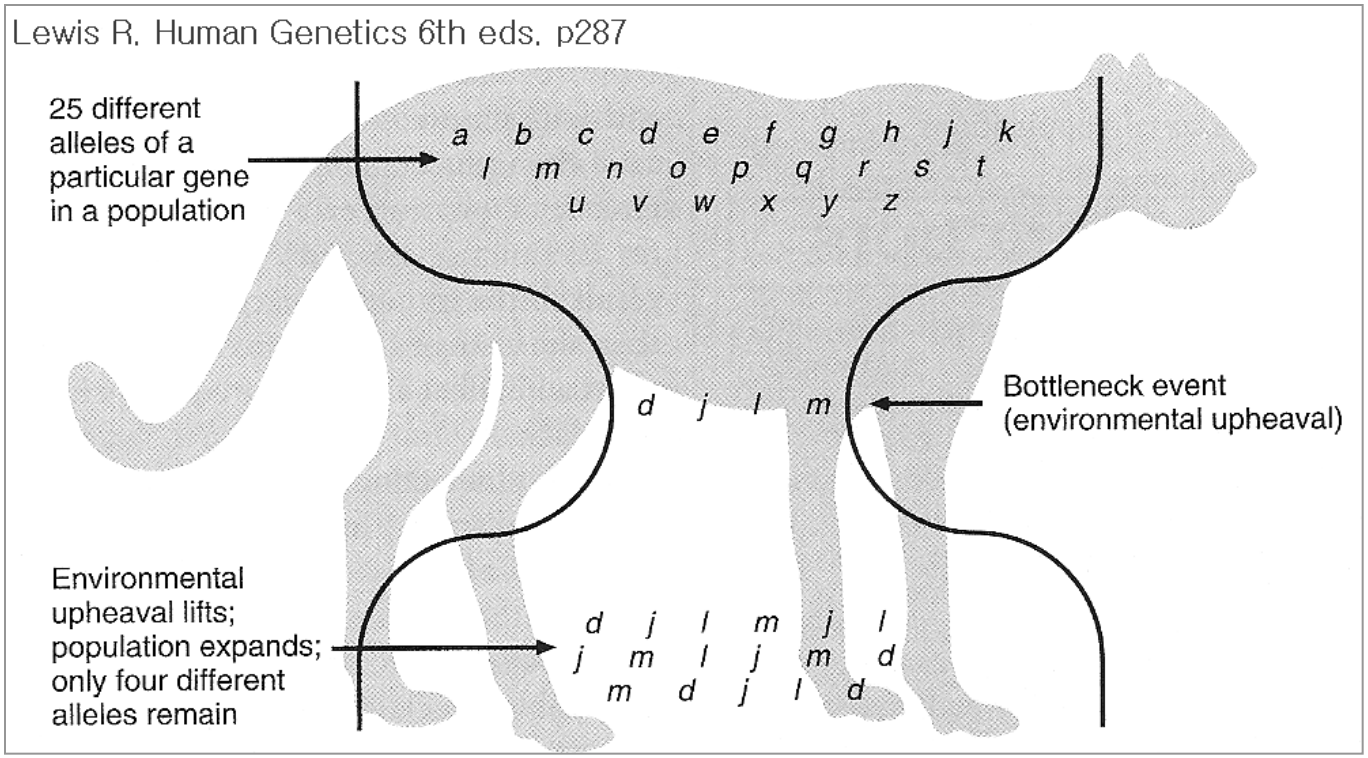

Lewis R. Human Genetics 6th eds. p287

요약 - 해상도

- 디지털 이미지의 정보는 pixel의 수로 결정된다.
- 이미지의 정보양을 증가시킬 방법은 없다.
- 이미지의 변형은 항상 해상도의 저하를 동반한다. 원본이미지를 확실하게 보관하자.

- 질문: 그래픽 이미지에는 항상 해상도가 있나요?

Topic 3

Vector image란 무엇인가?

성균관대학교 의과대학 삼성서울병원 내과 이준행

Digital camera로 찍은 image는 전형적인 bitmap image다.
확대를 하지 않으면 매우 자연스럽게 보인다.

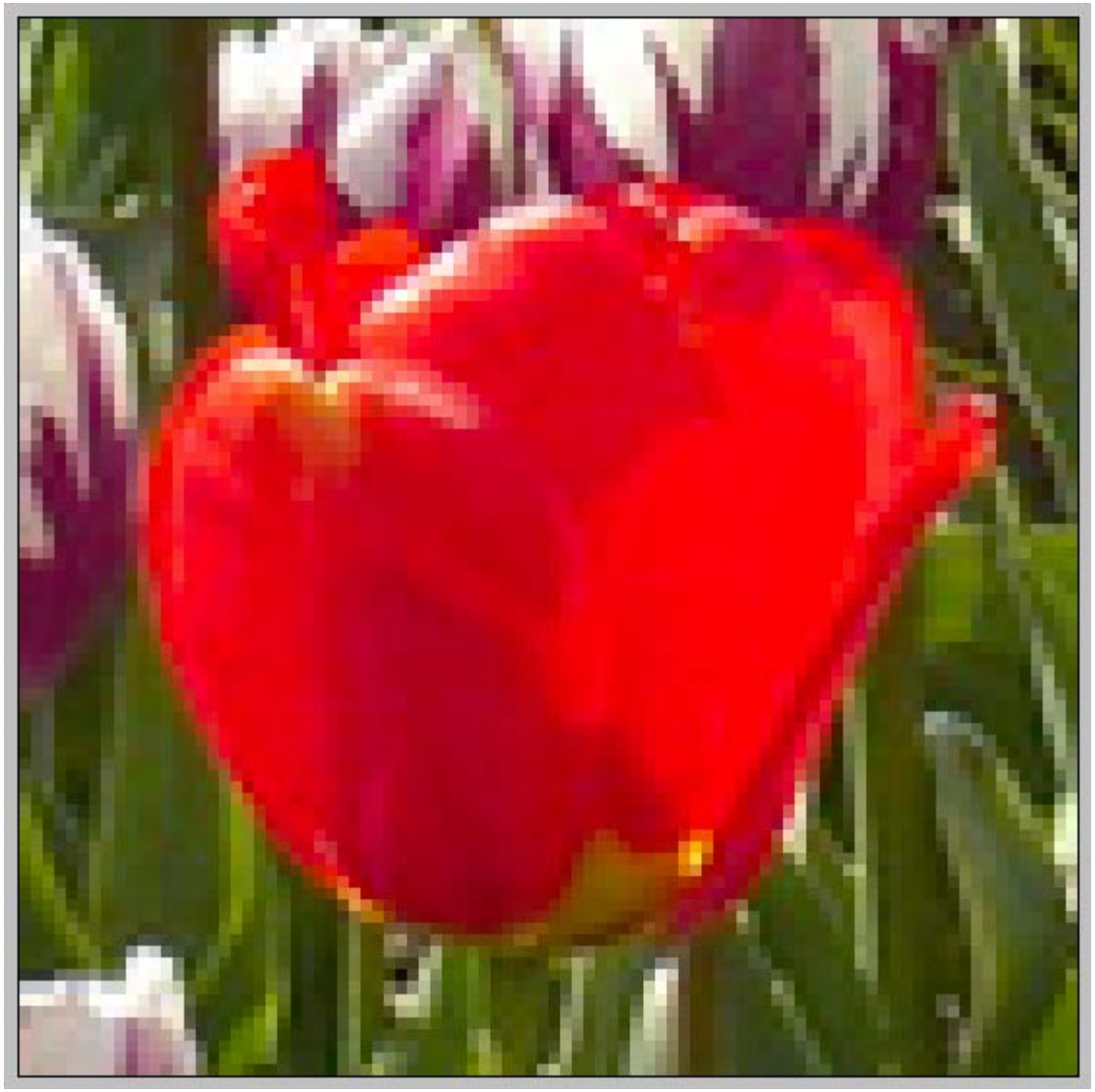

Pixel이 보이도록 크게 확대하면 격자구조를 볼 수 있다.

선을 그리는 두 가지 방법

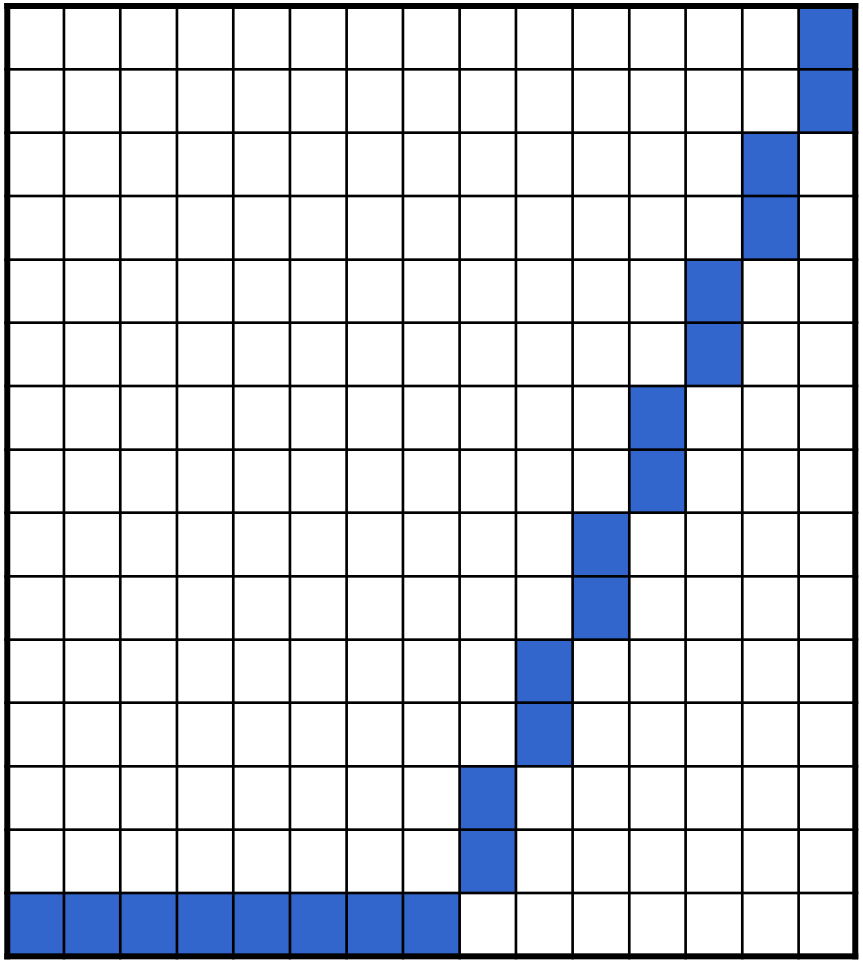

Bitmap (=rastor) image

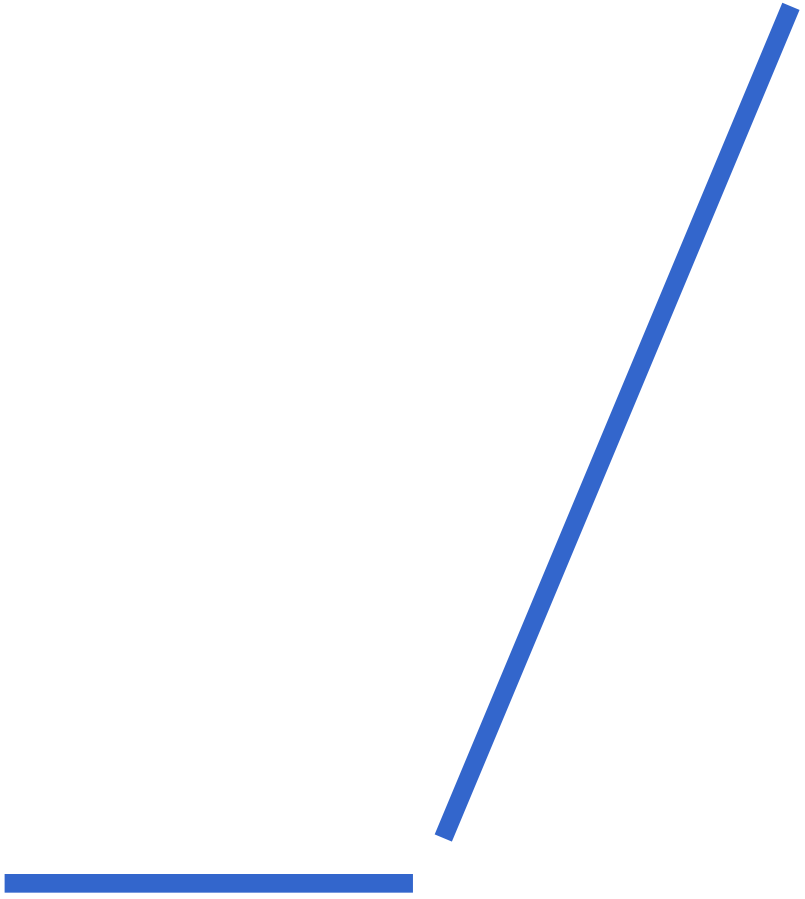

Vector image

Raster image (=bitmap image)

- A “raster” is a grid-like organization of image elements.
- Standard raster format: TIFF
- Raster image file has all the information for every pixel (picture element).

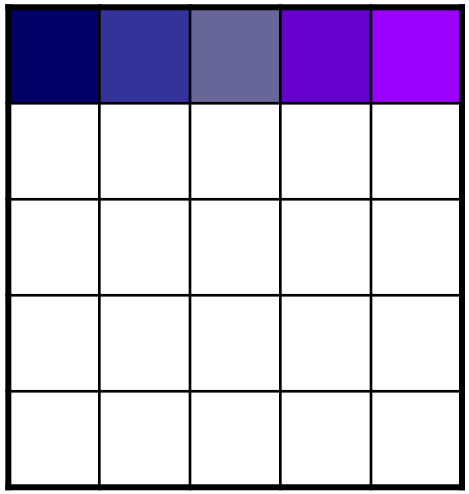

Is my image a vector file?

To ensure that your image is a vector drawing please conduct the following test:

1 In the document zoom in to the diagram 500% or more.

2 Check if lines such as curves have lost any quality, are appearing pixelated (made up of small squares rather than clear

3 If they are same file mentione check that

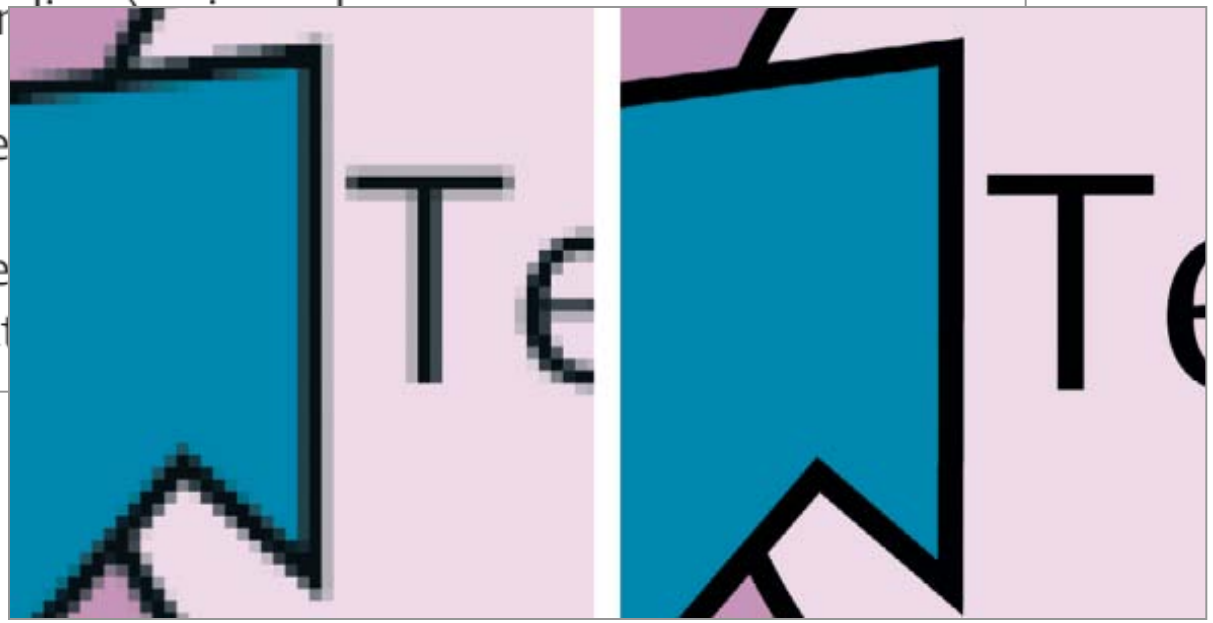

http://www.thelancet.com/webfiles/images/clusters/thelancet/EESartwork.pdf

우리가 흔히 사용하는 format은 대부분 bitmap (=rastor) image file format이다

File Format	Pertinent Application
DICOM	PACS
JPEG	PowerPoint, web-based display
TIFF	Print output, journal publication
PSD	Print output, when arrows or labels are necessary
GIF	Web-based display
EPS	Vector graphics
PDF	Distribution, web-based or otherwise
PICT	Some Macintosh applications use this format though it is largely replaced by the other formats
PNG	New format, may replace JPEG eventually

Note.—PICT = PICTure; PNG = portable networks graphics; PSD = PhotoShop document.

LaBerge. J Vasc Interv Radiol 2003;14:1223-1229

Some journals may requires vector drawings

Accepted file types

- For graphs and diagrams we prefer to accept vector drawings. These files would ideally be created in a program such as Adobe Illustrator or Corel Draw and saved as an encapsulated postscript (**.eps**) or portable document format (**.pdf**) files for uploading on-line.

- Other accepted vector files are Corel Draw (**.cdt**) and Adobe Illustrator (**.ai**). Please email these directly to the article editor as these formats are not supported for uploading.

http://www.thelancet.com/webfiles/images/clusters/thelancet/EESartwork.pdf

Selecting programs for vector images

- 우리가 사용하는 프로그램/도구는 대부분 bitmap임

- Bitmap (=raster) image
  - Photoshop
  - Cameras
  - Scanners
- Vector image
  - **Adobe illustrator**
  - Corel draw

Making a vector file in Prism

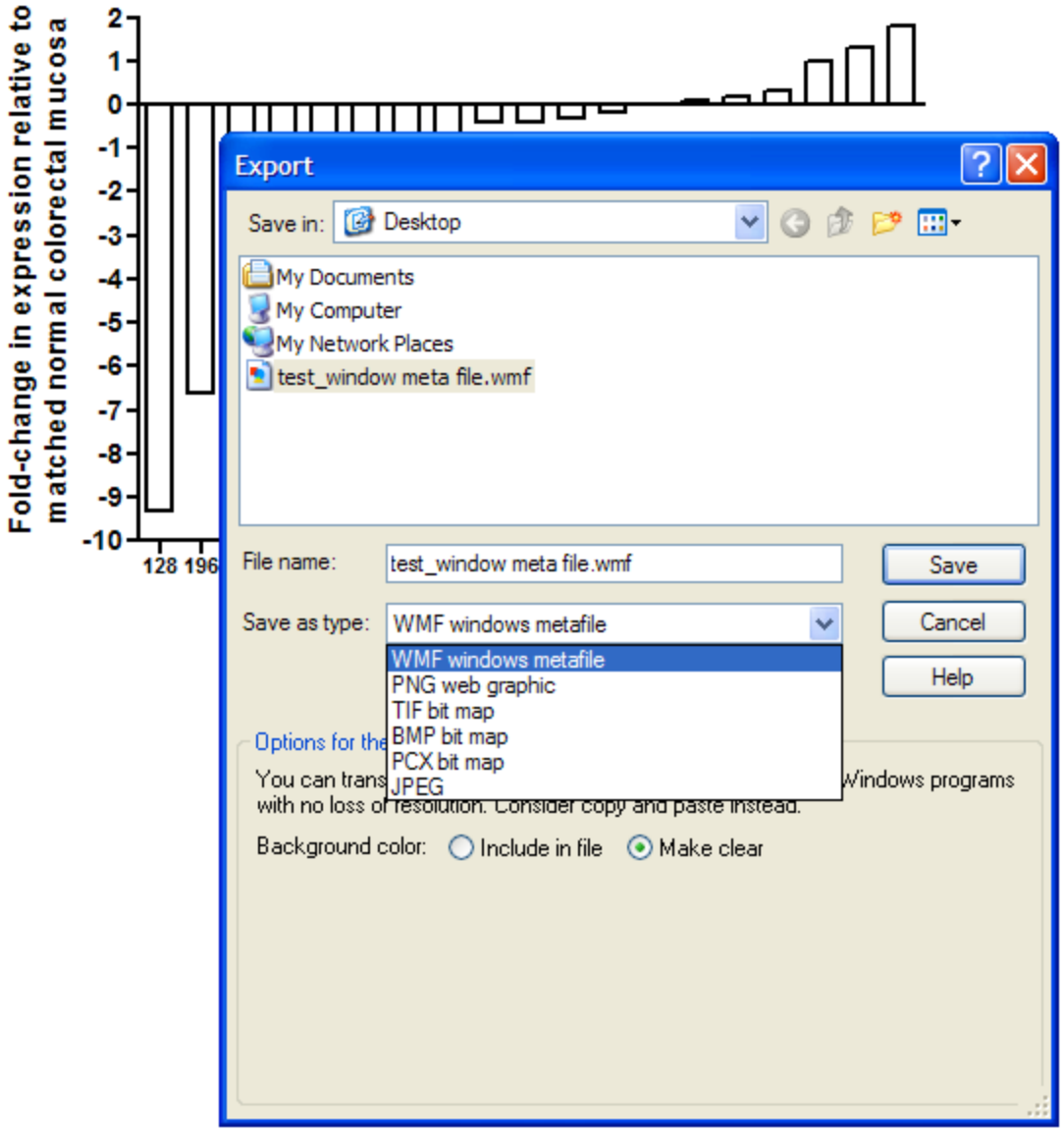

Insertion of the WMF file

- File size: 5,158 bytes

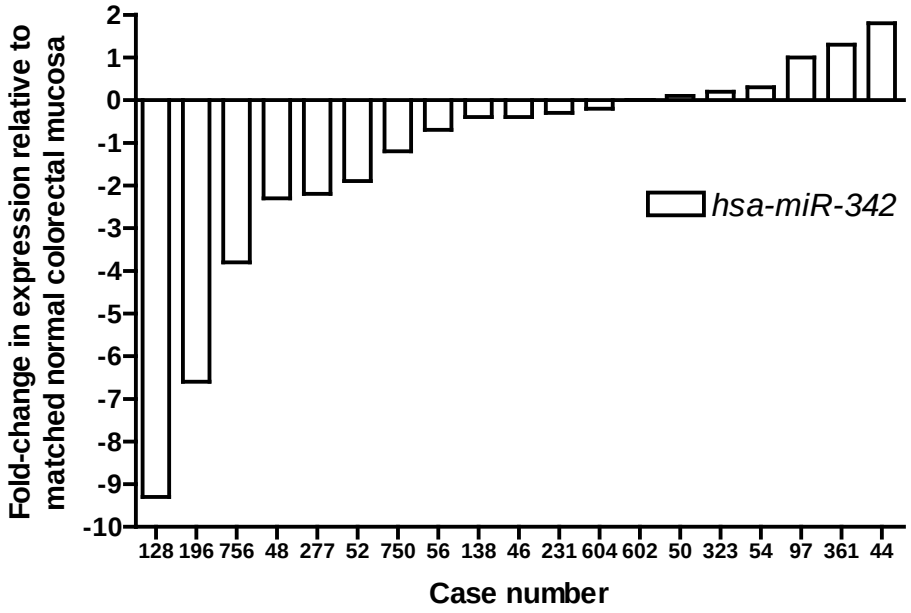

Windows Metafile (WMF) is a vector graphics format which also allows the inclusion of raster graphics.

X10 enlargement of the inserted WMF file

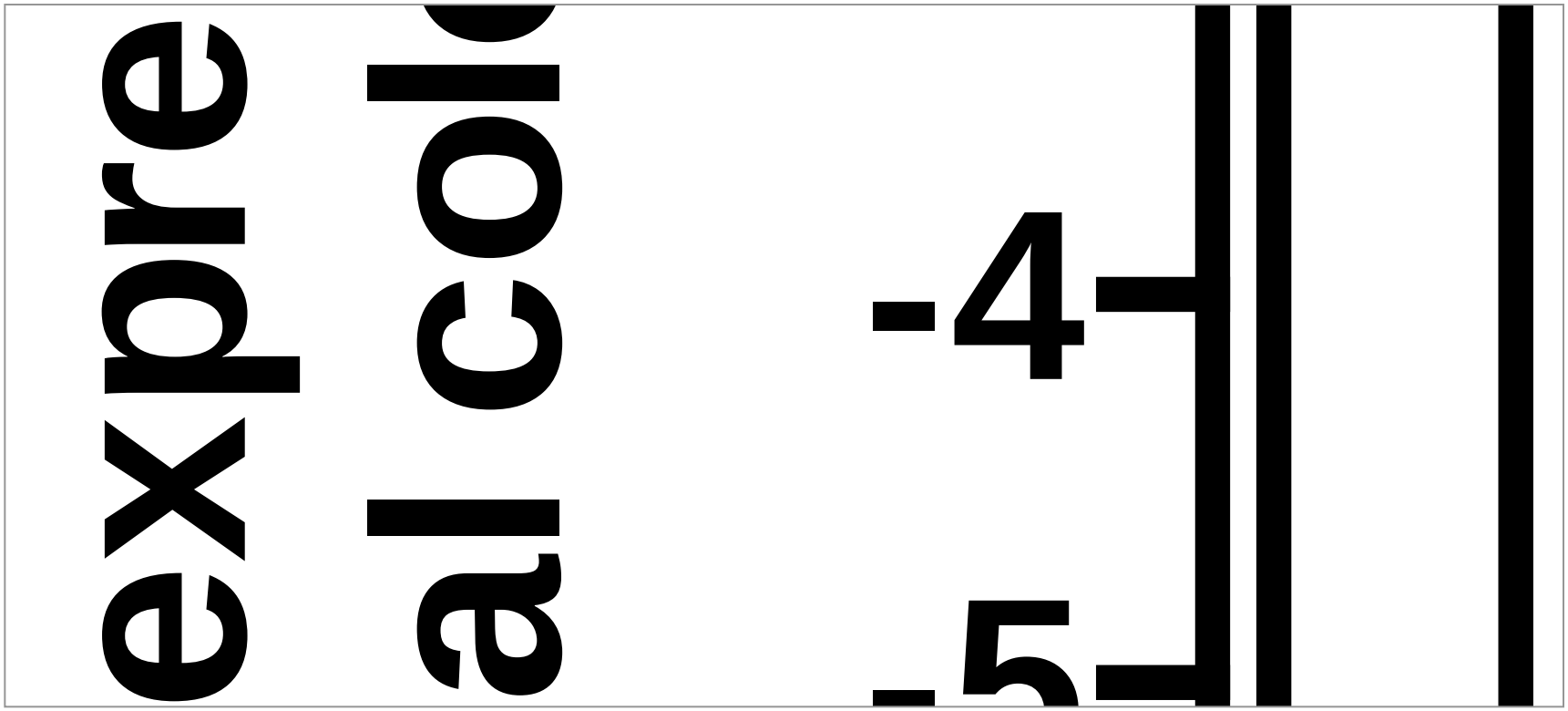

X100 enlargement of the inserted WMF file

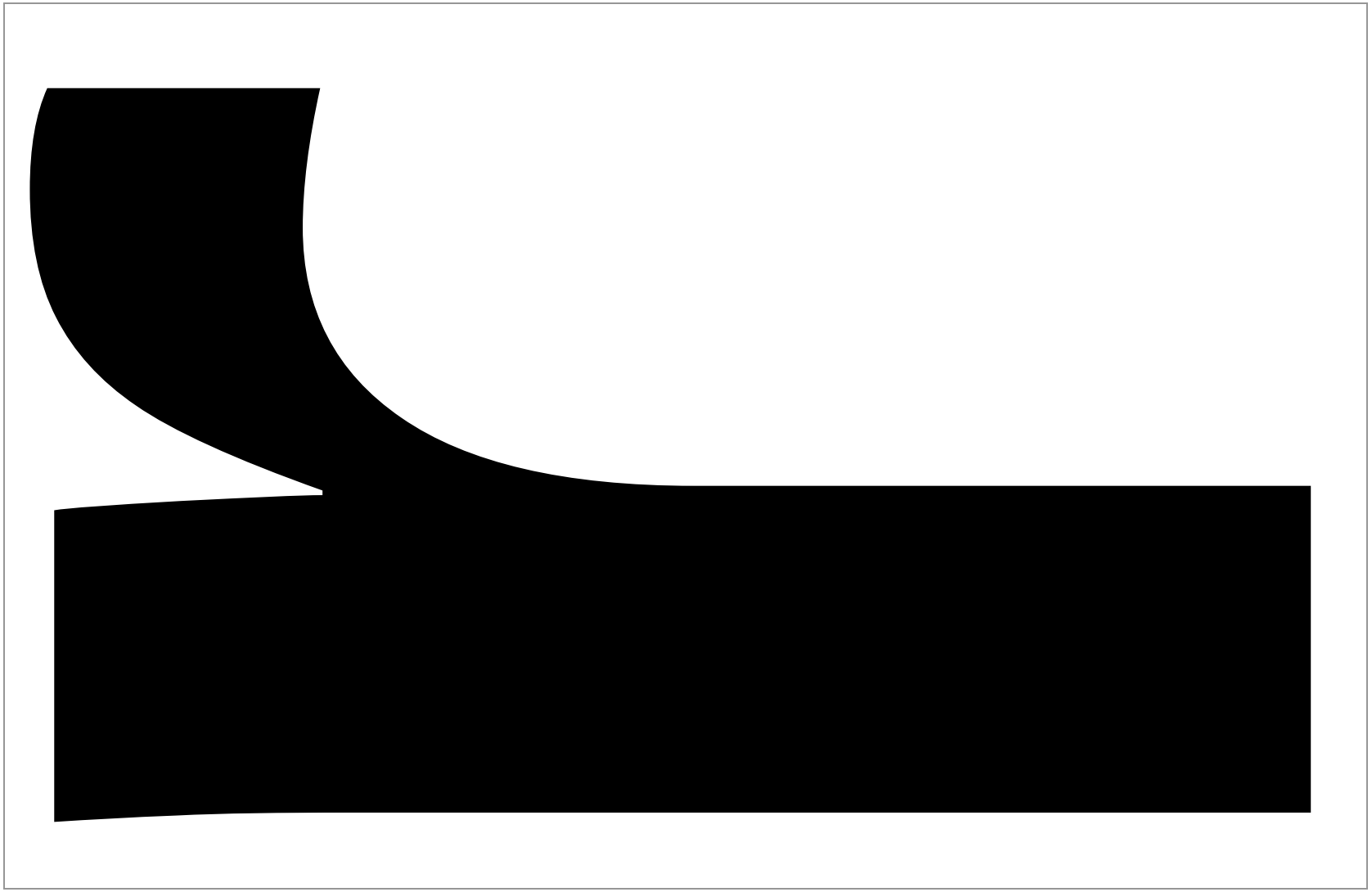

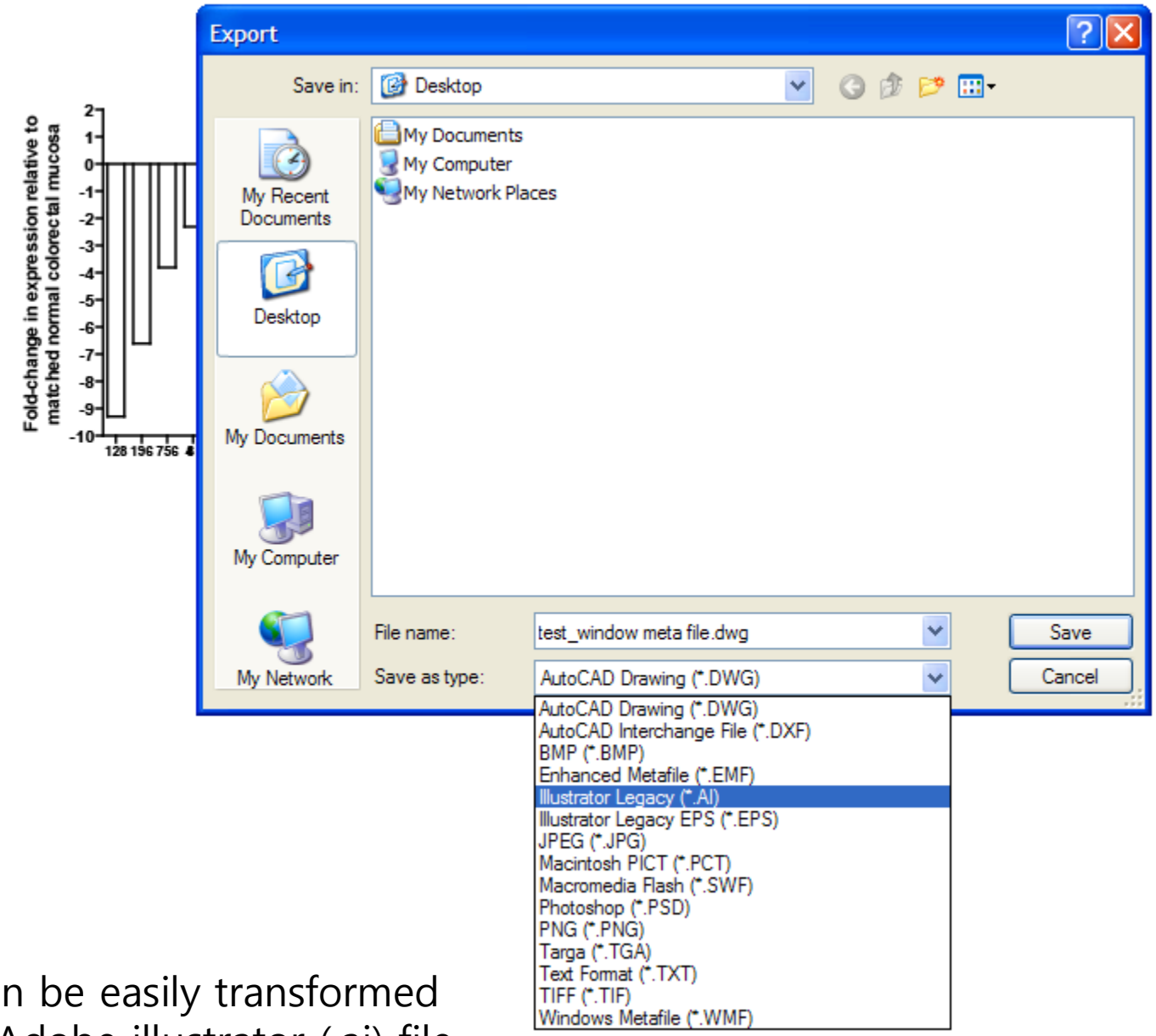

WMF can be easily transformed into an Adobe illustrator (.ai) file.

PowerPoint에서 구현하는 vector

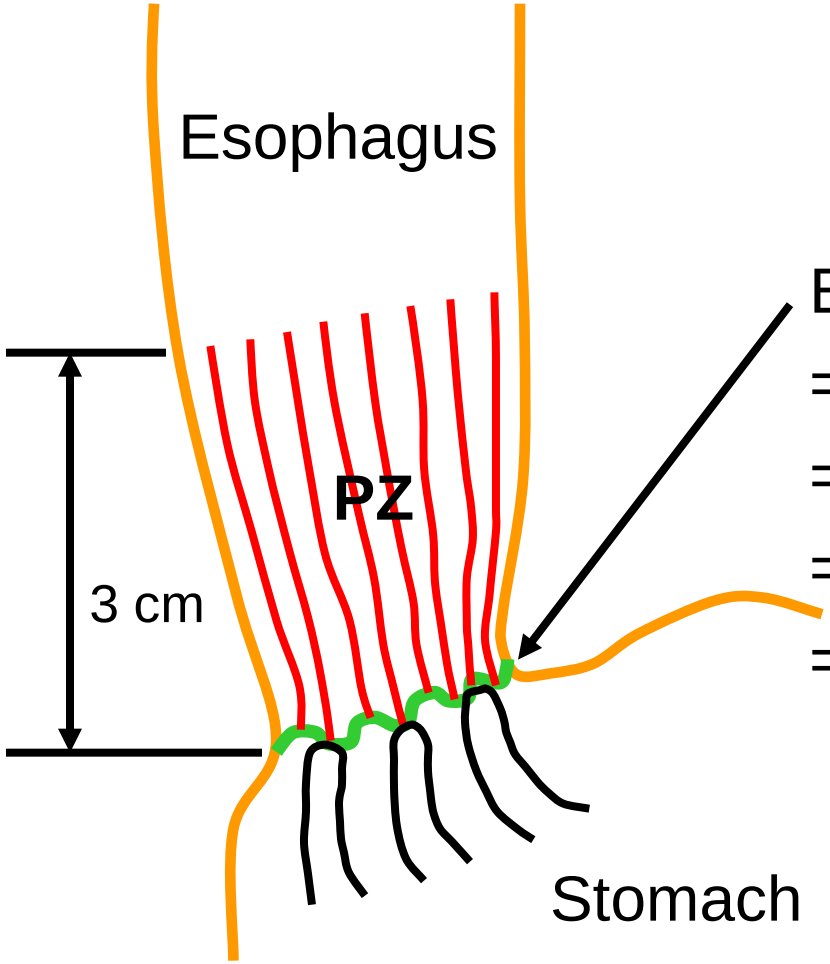

Esophagogastric junction (EGJ)
= Proximal margin of gastric folds
= Distal end of palisade zone
= Pinchcock action (PCA)
= Squamocolumnar junction

요약: vector image

- 선을 그리는 방법은 두 가지: Rastor와 vector
- Vector에서는 확대하여도 격자구조가 발생하지 않는다.
- 최고의 해상도를 얻기 위해서는 vector program을 이용하여 figure를 작성한 후 마지막에 필요한 해상도의 bitmap 파일로 변경하는 것이 좋다.

Topic 3

논문 제출을 위한 적절한 해상도?

성균관대학교 의과대학 삼성서울병원 내과 이준행

출판을 위한 해상도 선정 원칙

- Color: 300 dpi
- Gray scale: 300 - 600 dpi [required for photos, without text]
- Combination art (combo): 600 - 900 dpi [required for photos and text]
- Line art (monochrome 1-bit image): 900 - 1200 dpi [B&W text only]

DPI = Dots / Inch

최종 편집된 페이지에서 어떤 크기?

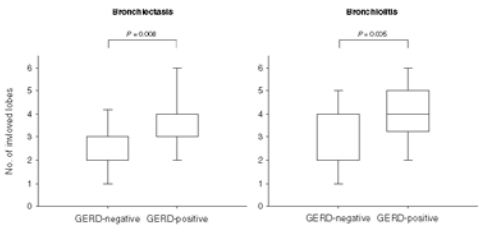

FIGURE 1. Box-and-whiskers graph of the quantitative imaging analysis showing the number of involved lobes with bronchiectasis and bronchiolitis. Bronchiolitis is defined as the presence of centrilobular small nodules (< 10 mm in diameter) or branching nodular structures (tree-in-bud pattern) on HRCT. The ends of the boxes indicate the 25th and 75th percentiles, and the lines in the bars indicate the median value. The 10th and 90th percentiles are indicated with whiskers. In the patients without GERD, the median numbers of involved lobes with bronchiectasis and bronchiolitis are both 2. In the patients with GERD, the median numbers of involved lobes with bronchiectasis and bronchiliitis are both 4. Bronchiectasis and bronchiolitis were observed in more lobes in pateints with GERD than in patients without GERD (p = 0.008 and p = 0.009, respectively).

In addition, patients with GERD were more likely to have AFB-positive sputum smear results in comparison with patients without GERD. These findings suggest that further studies to investigate the nature of the association between GERD and NTM lung disease are needed. If GERD is causative, its treatment may be critical. If GERD is secondary to more advanced lung disease, its treatment may be less important in managing the lung disease.

Our study had some limitations. First, this study did not include a control group. However, our principal goal was to investigate the prevalence of GERD in patients with the nodular bronchiectatic form of NTM lung disease, and ours is the only study to use 24-h pH monitoring to determine this.

Second, a significant proportion (34 of 92 patients, 37%) of screened patients did not perform 24-h esophageal pH monitoring. Then, the study group did not accurately reflect total population of patients with NTM lung disease. In particular, the study group had a significantly higher proportion of patients with *M abscessus* infection than the total group. This is very significant because it has been shown that patients with *M abscessus* infection have a higher rate of gastroesophageal abnormalities.

Third, we used accepted criteria used by gastroenterologists for the diagnosis of CERD, but these may not apply for a person to be susceptible to NTM infection by possible aspiration. For example, it is not known if someone has to have a pH
4 for > 4% of the study time to place NTM in his or her lungs. Also, the patients were only studied for 24 h, which does not exclude that aspiration may have occurred at other times not studied.

Although we showed that GERD is prevalent in patients with NTM lung disease, the nature of this relationship remains uncertain. Our study was not designed to investigate a possible causal association between GERD and NTM lung disease. Our data are consistent with GERD causing or contributing to the development or progression of NTM lung disease via recurrent exposure of the pulmonary parenchyma to the acidity of the refluxed gastric contents. Alternatively, GERD might be a secondary phenomenon. Patients with NTM lung disease might be at increased risk for abnormal reflux because of the increased pressure gradient across the diaphragm during frequent coughing and changes in pulmonary mechanics.

In addition, non-acid reflux as well as acid reflux may be present in patients with NTM lung disease. The measurement of acid reflux using esophageal pH monitoring is just a marker for possible aspiration but may not be related to the pathogenesis of NTM infection. In fact, it is possible that the increased use of acid suppressants with a resultant aspiration of relative alkaline pH into the esophagus may actually make the environment more favorable to NTM infection and the relative alkaline pH exacerbate further aspiration.

In conclusion, our study showed that patients with the nodular bronchiectatic form of NTM lung disease have a high prevalence of GERD. However, most patients with NTM lung disease and GERD lacked the typical symptoms of heartburn and regur-

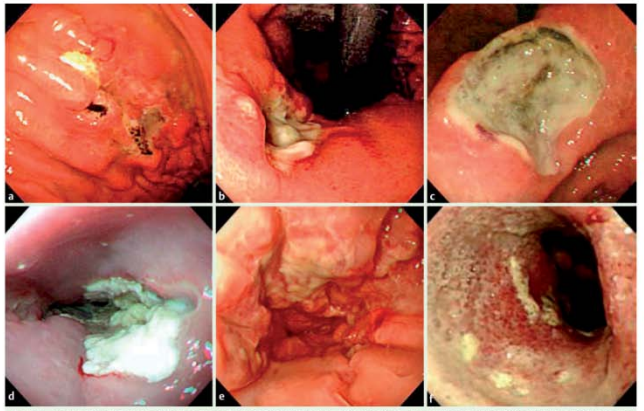

Figure 1 Endoscopic appearances of primary upper gastrointestinal NK-/T-cell lymphoma. **a** Superficial/erosive type (patient 1): several superficial erosions of various sizes in a continuous focal pattern in the body of the stomach. **b** Ulcerative type (patient 2): a round 1.5-cm well defined deep ulcer in the body of the stomach. **c** Ulcerative type (patient 3): round 2-cm well defined deep ulcer at the angle of the stomach. **d** Ulcerative type (patient 4): a long irregular 4-cm well defined deep ulcer in the mid esophagus. **e** Ulceroinfiltrative type (patient 5): diffuse ill defined ulcers of various sizes in a continuous pattern in the lower esophagus. **f** Ulceroinfiltrative type (patient 6): diffuse ill defined ulcers of various sizes in a continuous pattern in the second portion of the duodenum.

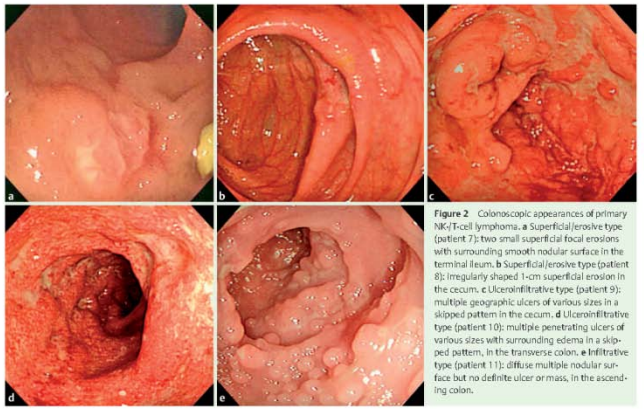

Figure 2 Colonoscopic appearances of primary NK-/T-cell lymphoma. **a** Superficial/erosive type (patient 7): two small superficial focal erosions with surrounding smooth nodular surface in the terminal ileum. **b** Superficial/erosive type (patient 8): irregularly shaped 1-cm superficial erosion in the cecum. **c** Ulceroinfiltrative type (patient 9): multiple geographic ulcers of various sizes in a skipped pattern in the cecum. **d** Ulceroinfiltrative type (patient 10): multiple penetrating ulcers of various sizes with surrounding edema in a skipped pattern, in the transverse colon. **e** Infiltrative type (patient 11): diffuse multiple nodular surface but no definite ulcer or mass, in the ascending colon.

매우 불친절한 *Science* 투고규정

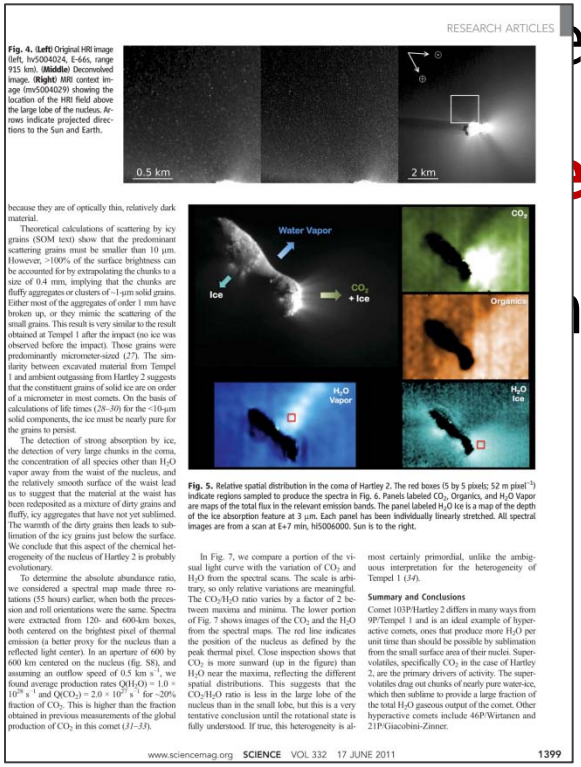

RESEARCH ARTICLES

Fig. 4. (Left) Original HRI image (left, hv5004024, E-66s, range 915 km). **(Middle)** Deconvolved image. **(Right)** HRI context image (mv5004029) showing the location of the HRI field above the large lobe of the nucleus. Arrows indicate projected directions to the Sun and Earth.

0.5 km

2 km

because they are of optically thin, relatively dark material.

Theoretical calculations of scattering by icy grains (SOM text) show that the predominant scattering grains must be smaller than 10 μm. However, 90% of the surface brightness can be accounted for by extrapolating the chunks to a size of 0.4 mm, implying that the chunks are fluffy aggregates or clusters of ~1-μm solid grains. Either most of the aggregates of order 1 mm have broken up, or they mimic the scattering of the small grains. This result is very similar to the result obtained at Tempel 1 after the impact (no ice was observed before the impact). Those grains were predominantly micrometer-sized (*27*). The similarity between excavated material from Tempel 1 and ambient outgassing from Hartley 2 suggests that the constituent grains of solid ice are on order of a micrometer in most comets. On the basis of calculations of life times (*28*–*30*) for the <10-μm solid components, the ice must be nearly pure for the grains to persist.

The detection of strong absorption by ice, the detection of very large chunks in the coma, the concentration of all species other than H_2O vapor away from the waist of the nucleus, and the relatively smooth surface of the waist lead us to suggest that the material at the waist has been redeposited as a mixture of dirty grains and fluffy, icy aggregates that have not yet sublimed. The warmth of the dirty grains then leads to sublimation of the icy grains just below the surface. We conclude that this aspect of the chemical heterogeneity of the nucleus of Hartley 2 is probably evolutionary.

To determine the absolute abundance ratio, we considered a spectral map made three rotations (55 hours) earlier, when both the precession and roll orientations were the same. Spectra were extracted from 120- and 600-km boxes, both centered on the brightest pixel of thermal emission (a better proxy for the nucleus than a reflected light center). In an aperture of 600 by 600 km centered on the nucleus (fig. S8), and assuming an outflow speed of 0.5 km s^{-1}, we found average production rates $Q(H_2O) = 1.0 \times 10^{28}$ s^{-1} and $Q(CO_2) = 2.0 \times 10^{27}$ s^{-1} for ~20% fraction of CO_2. This is higher than the fraction obtained in previous measurements of the global production of CO_2 in this comet (*31*–*33*).

Fig. 5. Relative spatial distribution in the coma of Hartley 2. The red boxes (5 by 5 pixels; 52 m $pixel^{-1}$) indicate regions sampled to produce the spectra in Fig. 6. Panels labeled CO_2, Organics, and H_2O Vapor are maps of the total flux in the relevant emission bands. The panel labeled H_2O Ice is a map of the depth of the ice absorption feature at 3 μm. Each panel has been individually linearly stretched. All spectral images are from a scan at E+7 min, hi5006000. Sun is to the right.

In Fig. 7, we compare a portion of the visual light curve with the variation of CO_2 and H_2O from the spectral scans. The scale is arbitrary, so only relative variations are meaningful. The CO_2/H_2O ratio varies by a factor of 2 between maxima and minima. The lower portion of Fig. 7 shows images of the CO_2 and the H_2O from the spectral maps. The red line indicates the position of the nucleus as defined by the peak thermal pixel. Close inspection shows that CO_2 is more sunward (up in the figure) than H_2O near the maxima, reflecting the different spatial distributions. This suggests that the CO_2/H_2O ratio is less in the large lobe of the nucleus than in the small lobe, but this is a very tentative conclusion until the rotational state is fully understood. If true, this heterogeneity is almost certainly primordial, unlike the ambiguous interpretation for the heterogeneity of Tempel 1 (*34*).

Summary and Conclusions

Comet 103P/Hartley 2 differs in many ways from 9P/Tempel 1 and is an ideal example of hyperactive comets, ones that produce more H_2O per unit time than should be possible by sublimation from the small surface area of their nuclei. Supervolatiles, specifically CO_2 in the case of Hartley 2, are the primary drivers of activity. The supervolatiles drag out chunks of nearly pure water-ice, which then sublime to provide a large fraction of the total H_2O gaseous output of the comet. Other hyperactive comets include 46P/Wirtanen and 21P/Giacobini-Zinner.

RESEARCH ARTICLES

O-Glycosylated Cell Wall Proteins Are Essential in Root Hair Growth

Silvia M. Velasquez,[1] Martiniano M. Ricardi,[1] Javier Gloazzo Dorosz,[1] Paula V. Fernandez,[2] Alejandro D. Nadra,[3] Laercio Pol-Fachin,[4] Jack Egelund,[5] Sascha Gille,[6] Jesper Harholt,[7] Marina Ciancia,[2] Hugo Verli,[4] Markus Pauly,[6] Antony Bacic,[8] Carl Erik Olsen,[9] Peter Ulvskov,[5] Bent Larsen Petersen,[5] Chris Somerville,[6] Norberto D. Iusem,[1,10] Jose M. Estevez[1]*

Root hairs are single cells that develop by tip growth and are specialized in the absorption of nutrients. Their cell walls are composed of polysaccharides and hydroxyproline-rich glycoproteins (HRGPs) that include extensins (EXTs) and arabinogalactan-proteins (AGPs). Proline hydroxylation, an early posttranslational modification of HRGPs that is catalyzed by prolyl 4-hydroxylases (P4Hs), defines the subsequent O-glycosylation sites in EXTs (which are mainly arabinosylated) and AGPs (which are mainly arabinogalactosylated). We explored the biological function of P4Hs, arabinosyltransferases, and EXTs in root hair cell growth. Biochemical inhibition or genetic disruption resulted in the blockage of polarized growth in root hairs and reduced arabinosylation of EXTs. Our results demonstrate that correct O-glycosylation on EXTs is essential for cell-wall self-assembly and, hence, root hair elongation in *Arabidopsis thaliana*.

Plant cell walls are complex and dynamic structures composed mostly of high-molecular-weight polysaccharides and highly glycosylated proteins (*1*, *2*). During plant growth, cells may expand up to 200 times their original length. During this process, the cell wall maintains its thickness through the addition of newly synthesized polysaccharides and proteins. Therefore, walls must possess sufficient tensile strength to withstand enormous turgor pressures (the driving force for growth) and involves controlled chemical modifications of wall constituents and wall networks. Approximately 1 to 2% of the *Arabidopsis* genome represents genes encoding putative enzymes that catalyze such modifications (*2*). Although the catalytic activity of the encoded protein is inferred from the predicted peptide sequence, the precise enzymatic function and biological role of many of these putative cell wall–modifying genes are unknown (*1*, *2*).

Cell walls contain abundant hydroxyproline-rich glycoproteins (HRGPs), a superfamily that encompasses extensins (EXTs) (*3*, *4*), proline-rich proteins (PRPs) (*4*), and arabinogalactan-proteins (AGPs) (*4*, *5*). These proteins undergo extensive posttranslational modification, which includes the modification of proline (Pro) residues to hydroxyproline (Hyp) by membrane-bound prolyl 4-hydroxylases (P4H2) (*6*). Nascent HRGPs are O-glycosylated (with arabinose and/or galactose) by glycosyltransferases (GTs) in the Golgi and endoplasmic reticulum (ER) (*7*–*11*) and are cross-linked into the wall by peroxidases through alternate Tyr residues to form a covalent network (*12*, *13*).

Root hair growth and proline hydroxylation. To study the function of HRGPs, we focused on root hairs because they represent a single cell type that plays an important role in nutrient absorption, and the growth morphology is easily

[1]Instituto de Fisiología, Biología Molecular y Neurociencias–Consejo Nacional de Investigaciones Científicas y Técnicas (IFIByNE-CONICET), Facultad de Ciencias Exactas y Naturales, Universidad de Buenos Aires, Buenos Aires C1428EGA, Argentina. [2]Cátedra de Química de Biomoléculas, Departamento de Biología Aplicada y Alimentos (Centro de Investigaciones en Hidratos de Carbono–CONICET), Facultad de Agronomía, Universidad de Buenos Aires, Buenos Aires CD14JTDSE, Argentina. [3]Departamento de Química Biológica, Facultad de Ciencias Exactas y Naturales, Universidad de Buenos Aires, Buenos Aires C1428EGA, Argentina. [4]Programa de Pos-Graduação em Biologia Celular e Molecular, Centro de Biotecnologia, 91500-979, and Faculdade de Farmácia, Universidade Federal do Rio Grande do Sul, 90610-000, Brazil. [5]Department of Plant Biology and Biotechnology, Faculty of Life Sciences, University of Copenhagen, Copenhagen 1871, Denmark. [6]Energy Biosciences Institute, University of California, Berkeley, Berkeley, CA 94720, USA. [7]Department of Plant Biology and Biotechnology, Faculty of Life Sciences, University of Copenhagen, Copenhagen 1871, Denmark. [8]Plant Cell Biology Research Centre, School of Botany, University of Melbourne, Melbourne VIC 3010, Australia. [9]Department of Natural Sciences, Bioorganic Chemistry, Faculty of Life Sciences, University of Copenhagen, 1871, Denmark. [10]Departamento de Fisiología, Biología Molecular y Celular, Laboratorio de Fisiología y Biología Molecular (UFBM), Facultad de Ciencias Exactas y Naturales, Universidad de Buenos Aires, Buenos Aires C1428EGA, Argentina.

*To whom correspondence should be addressed. E-mail: jestevez@fbmc.fcen.uba.ar

Fig. 1. *Arabidopsis* root hair growth is modulated by P4Hs. **(A)** Localization of GFP-tagged P4H2, P4H5, and P4H13 enzymes. GFP-tagged P4H2 and P4H5 are expressed in trichoblast cells (T), and GFP-tagged P4H13 is expressed in both trichoblast and atrichoblast (AT) root cells. Absence of GFP signal is indicated by asterisks. Scale bar, 200 μm. **(B)** Shorter root hairs in *p4h13* mutant. Scale bar, 800 μm. **(C)** Root hair length (black bars) and Hyp content (red bars) in roots of WT Col-0 (WT), *p4h* insertional mutants, silenced [artificial microRNA (amiRNA)], and rescued mutants. Complementation of each *p4h* mutant was achieved by the corresponding WT P4H driven by either its own endogenous promoter or the 35S promoter. *P* values of one-way analysis of variance (ANOVA) test, $*P < 0.01$, $**P < 0.001$.

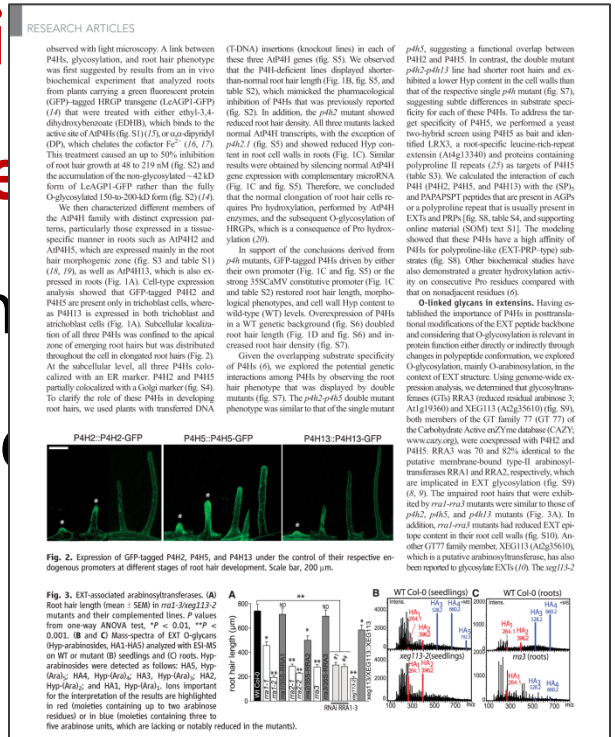

RESEARCH ARTICLES

observed with light microscopy. A link between P4Hs, glycosylation, and root hair phenotype was first suggested by results from an in vivo biochemical experiment that analyzed roots from plants carrying a green fluorescent protein (GFP)–tagged HRGP transgene (LeAGP1-GFP) (*14*) that were treated with either ethyl-3,4-dihydroxybenzoate (EDHB), which binds to the active site of AtP4Hs (fig. S1) (*15*), or α,α-dipyridyl (DP), which chelates the cofactor Fe^{2+} (*16*, *17*). This treatment caused an up to 50% inhibition of root hair growth at 48 to 219 nM (fig. S2) and the accumulation of the non-glycosylated ~42 kD form of LeAGP1-GFP rather than the fully O-glycosylated 150-to-200-kD form (fig. S2) (*14*).

We then characterized different members of the AtP4H family with distinct expression patterns, particularly those expressed in a tissue-specific manner in roots such as AtP4H2 and AtP4H5, which are expressed mainly in the root hair morphogenic zone (fig. S3 and table S1) (*18*, *19*), as well as AtP4H13, which is also expressed in roots (Fig. 1A). Cell-type expression analysis showed that GFP-tagged P4H2 and P4H5 are present only in trichoblast cells, whereas P4H13 is expressed in both trichoblast and atrichoblast cells (Fig. 1A). Subcellular localization of all three P4Hs was confined to the apical zone of emerging root hairs but was distributed throughout the cell in elongated root hairs (Fig. 2). At the subcellular level, all three P4Hs colocalized with an ER marker. P4H2 and P4H5 partially colocalized with a Golgi marker (fig. S4). To clarify the role of these P4Hs in developing root hairs, we used plants with transferred DNA (T-DNA) insertions (knockout lines) in each of these three AtP4H genes (fig. S5). We observed that the P4H-deficient lines displayed shorter-than-normal root hair length (Fig. 1B, fig. S5, and table S2), which mimicked the pharmacological inhibition of P4Hs that was previously reported (fig. S2). In addition, the *p4h2* mutant showed reduced root hair density. All three mutants lacked normal AtP4H transcripts, with the exception of *p4h2.1* (fig. S5) and showed reduced Hyp content in root cell walls in roots (Fig. 1C). Similar results were obtained by silencing normal AtP4H gene expression with complementary microRNA (Fig. 1C and fig. S5). Therefore, we concluded that the normal elongation of root hair cells requires Pro hydroxylation, performed by AtP4H enzymes, and the subsequent O-glycosylation of HRGPs, which is a consequence of Pro hydroxylation (*20*).

In support of the conclusions derived from *p4h* mutants, GFP-tagged P4Hs driven by either their own promoter (Fig. 1C and fig. S5) or the strong 35SCaMV constitutive promoter (Fig. 1C and table S2) restored root hair length, morphological phenotypes, and cell wall Hyp content to wild-type (WT) levels. Overexpression of P4Hs in a WT genetic background (fig. S6) doubled root hair length (Fig. 1D and fig. S6) and increased root hair density (fig. S7).

Given the overlapping substrate specificity of P4Hs (*6*), we explored the potential genetic interactions among P4Hs by observing the root hair phenotype that was displayed by double mutants (fig. S7). The *p4h2-p4h5* double mutant phenotype was similar to that of the single mutant *p4h5*, suggesting a functional overlap between P4H2 and P4H5. In contrast, the double mutant *p4h2-p4h13* line had shorter root hairs and exhibited a lower Hyp content in the cell walls than that of the respective single *p4h* mutant (fig. S7), suggesting subtle differences in substrate specificity for each of these P4Hs. To address the target specificity of P4H5, we performed a yeast two-hybrid screen using P4H5 as bait and identified LRX3, a root-specific leucine-rich-repeat extensin (At4g13340) and proteins containing polyproline II repeats (*25*) as targets of P4H5 (table S3). We calculated the interaction of each P4H (P4H2, P4H5, and P4H13) with the (SP)$_5$ and PAPAPSPT peptides that are present in AGPs or a polyproline repeat that is usually present in EXTs and PRPs [fig. S8, table S4, and supporting online material (SOM) text S1]. The modeling showed that these P4Hs have a high affinity of P4Hs for polyproline-like (EXT-PRP-type) substrates (fig. S8). Other biochemical studies have also demonstrated a greater hydroxylation activity on consecutive Pro residues compared with that on nonadjacent residues (*6*).

O-linked glycans in extensins. Having established the importance of P4Hs in posttranslational modifications of the EXT peptide backbone and considering that O-glycosylation is relevant in protein function either directly or indirectly through changes in polypeptide conformation, we explored O-glycosylation, mainly O-arabinosylation, in the context of EXT structure. Using genome-wide expression analysis, we determined that glycosyltransferases (GTs) RRA3 (reduced residual arabinose 3; At1g19360) and XEG113 (At2g35610) (fig. S9), both members of the GT family 77 (GT 77) of the Carbohydrate Active enZYme database (CAZY; www.cazy.org), were coexpressed with P4H2 and P4H5. RRA3 was 70 and 82% identical to the putative membrane-bound type-II arabinosyltransferases RRA1 and RRA2, respectively, which are implicated in EXT glycosylation (fig. S9) (*8*, *9*). The impaired root hairs that were exhibited by *rra1-rra3* mutants were similar to those of *p4h2*, *p4h5*, and *p4h13* mutants (Fig. 3A). In addition, *rra1-rra3* mutants had reduced EXT epitope content in their root cell walls (fig. S10). Another GT77 family member, XEG113 (At2g35610), which is a putative arabinosyltransferase, has also been reported to glycosylate EXTs (*10*). The *xeg113-2*

Fig. 2. Expression of GFP-tagged P4H2, P4H5, and P4H13 under the control of their respective endogenous promoters at different stages of root hair development. Scale bar, 200 μm.

Fig. 3. EXT-associated arabinosyltransferases. **(A)** Root hair length (mean ± SEM) in *rra1-3/xeg113-2* mutants and their complemented lines. *P* values from one-way ANOVA test, $*P < 0.01$, $**P < 0.001$. **(B** and **C)** Mass-spectra of EXT O-glycans (Hyp-arabinosides, HA1-HA5) analyzed with ESI-MS on WT or mutant (B) seedlings and (C) roots. Hyp-arabinosides were detected as follows: HA5, Hyp-(Ara)$_5$; HA4, Hyp-(Ara)$_4$; HA3, Hyp-(Ara)$_3$; HA2, Hyp-(Ara)$_2$; and HA1, Hyp-(Ara)$_1$. Ions important for the interpretation of the results are highlighted in red (moieties containing up to two arabinose residues) or in blue (moieties containing three to five arabinose units, which are lacking or notably reduced in the mutants).

매우 친절한 *Lancet*

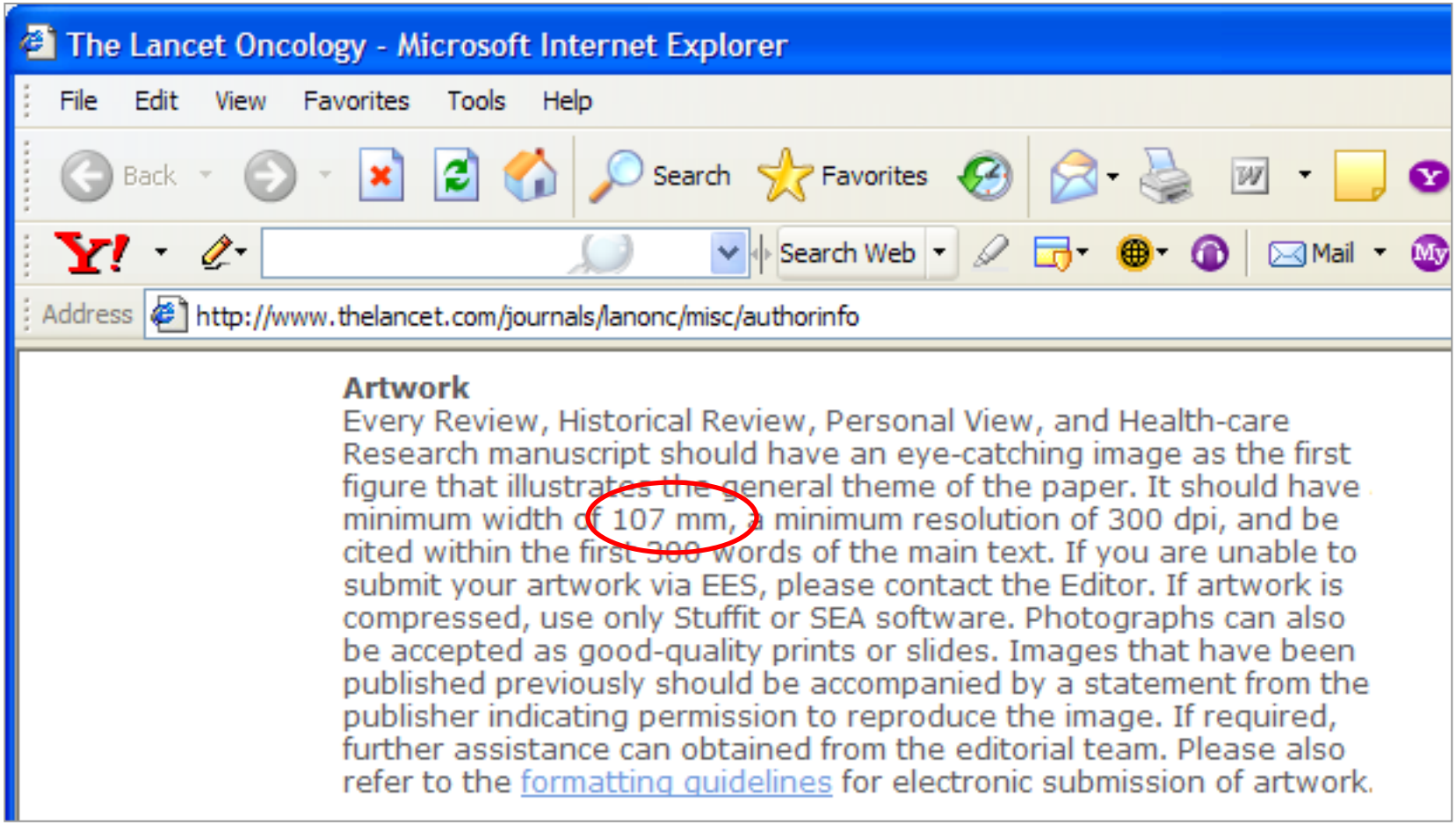

http://www.thelancet.com/journals/lanonc/misc/authorinfo

One column is usually 3.5 inch or less

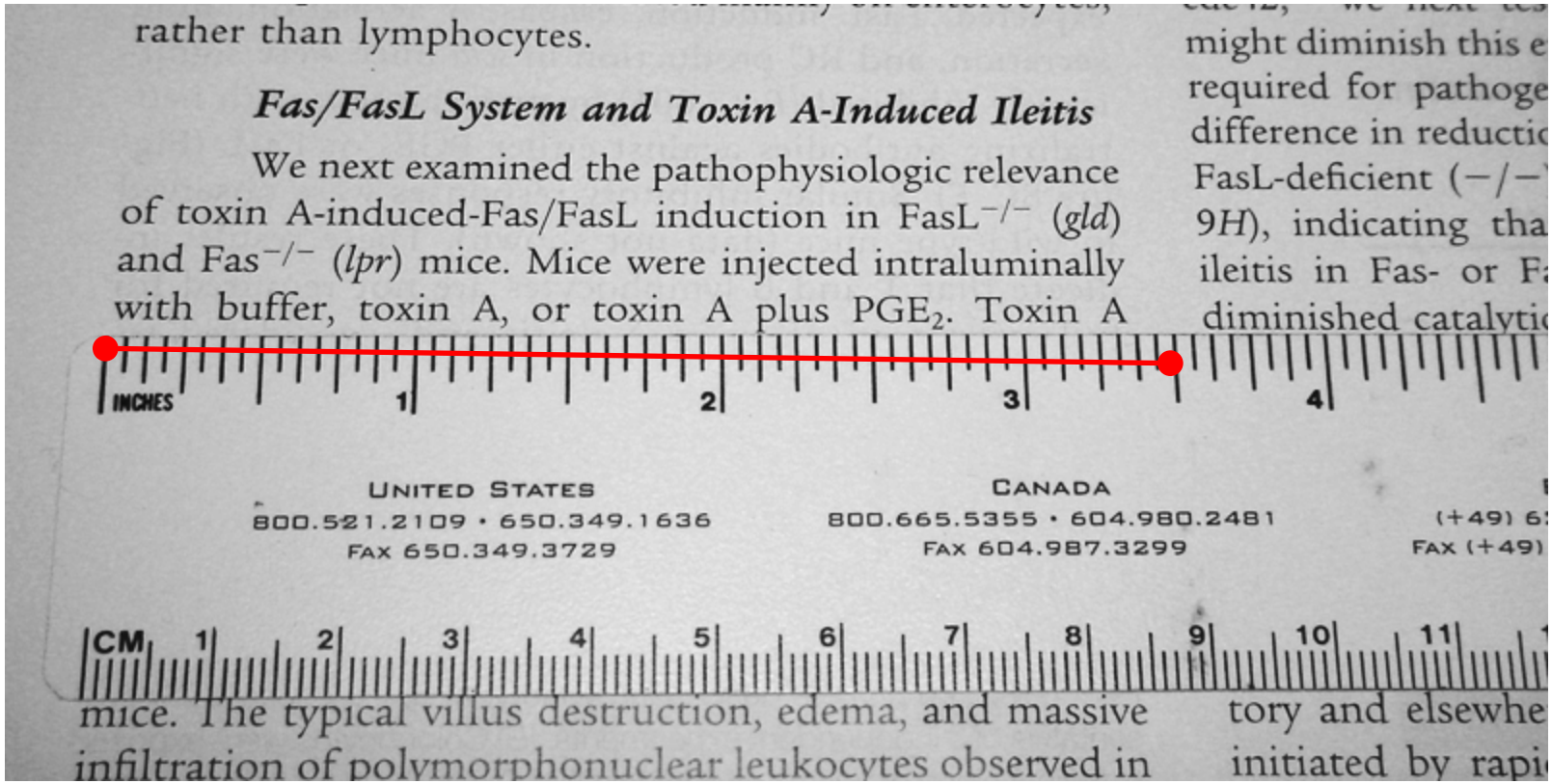

4 inch, 900 dpi로 작업을 하면 대부분의 경우에 문제가 없다

Kim. Gastroenterology 2007;133:875-886

대한 병리학회지 투고규정

- 2011/7 & 2014/7

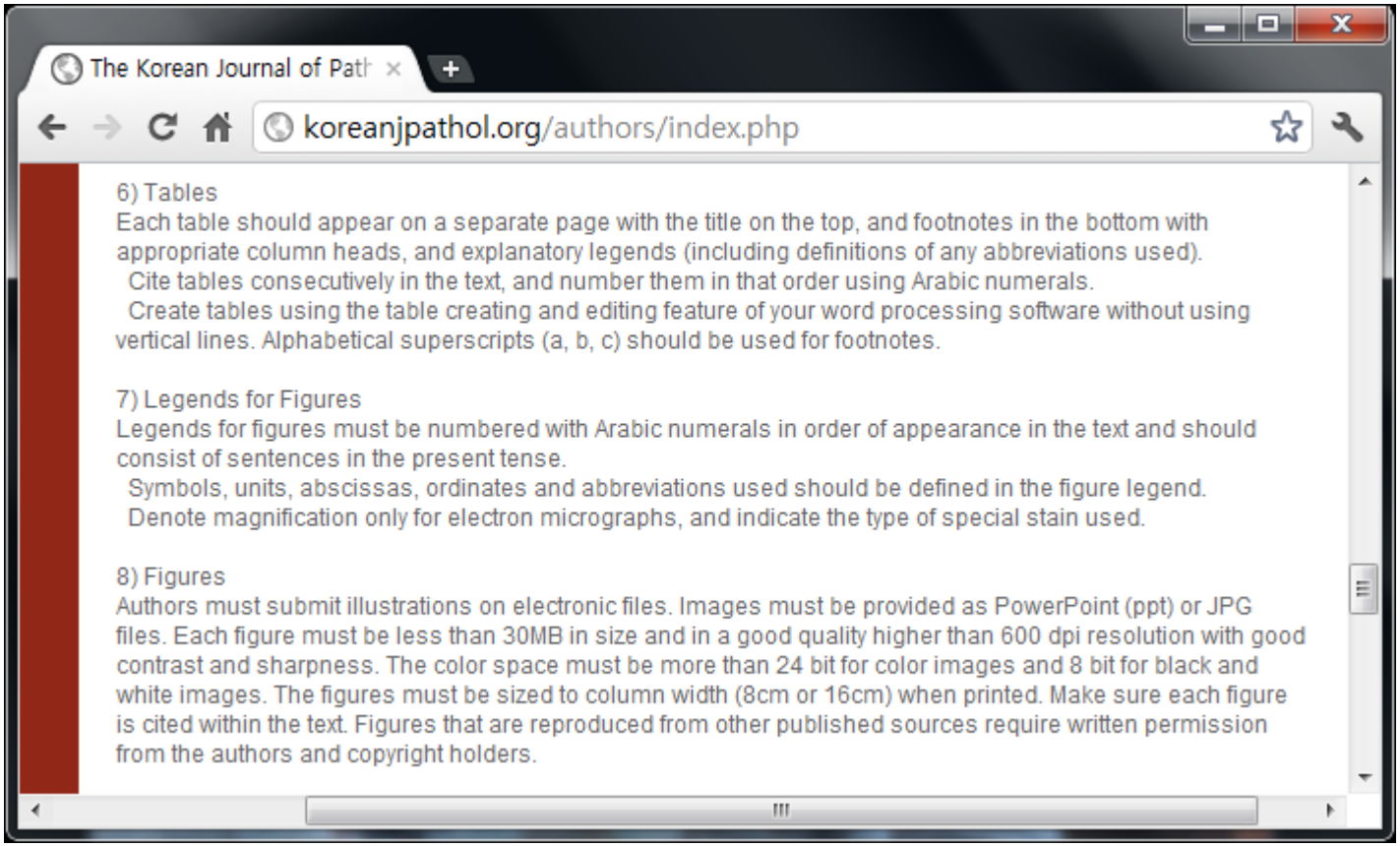

- Authors must submit illustrations on electronic files. Images must be provided as **PowerPoint (ppt) or JPG** files.
- Each figure must be less than **30MB in size** and in a good quality higher than **600 dpi** resolution with good contrast and sharpness.
- The **color space** must be more than 24 bit for color images and 8 bit for black and white images.
- The figures must be sized to column **width (8cm or 16cm)** when printed.

- Authors must submit illustrations on electronic files. Images must be provided as **TIFF files. JPEG is also acceptable when the original format is JPEG.**
- Each figure must be l~~ess than 30MB in size~~ and ~~in a~~ good quality higher than **300 dpi** resolution with good contrast and sharpness.
- ~~The **color space** must be more than 24 bit for color images and 8 bit for black and white images~~.
- The figures must be sized to **4 inches**.
- **If possible, submit the original file without any modification.**

요약: 논문 제출을 위한 이미지

- 논문에 제출할 그림은 대표적인 line art이다.
- 가능하면 vector형식의 image program을 사용하여 그림을 만드는 것이 좋다.
  예) 그림은 Adobe Illustrator, Graph는 Prism
- 마지막 단계에서 “TIFF 형식, size 4 inch, resolution 900 dpi, 색상 흑백” 선택

Tip

PowerPoint를 TIFF로 바꾸기

성균관대학교 의과대학 삼성서울병원 내과 이준행

PowerPoint에서 손쉽게 TIFF로 만들기

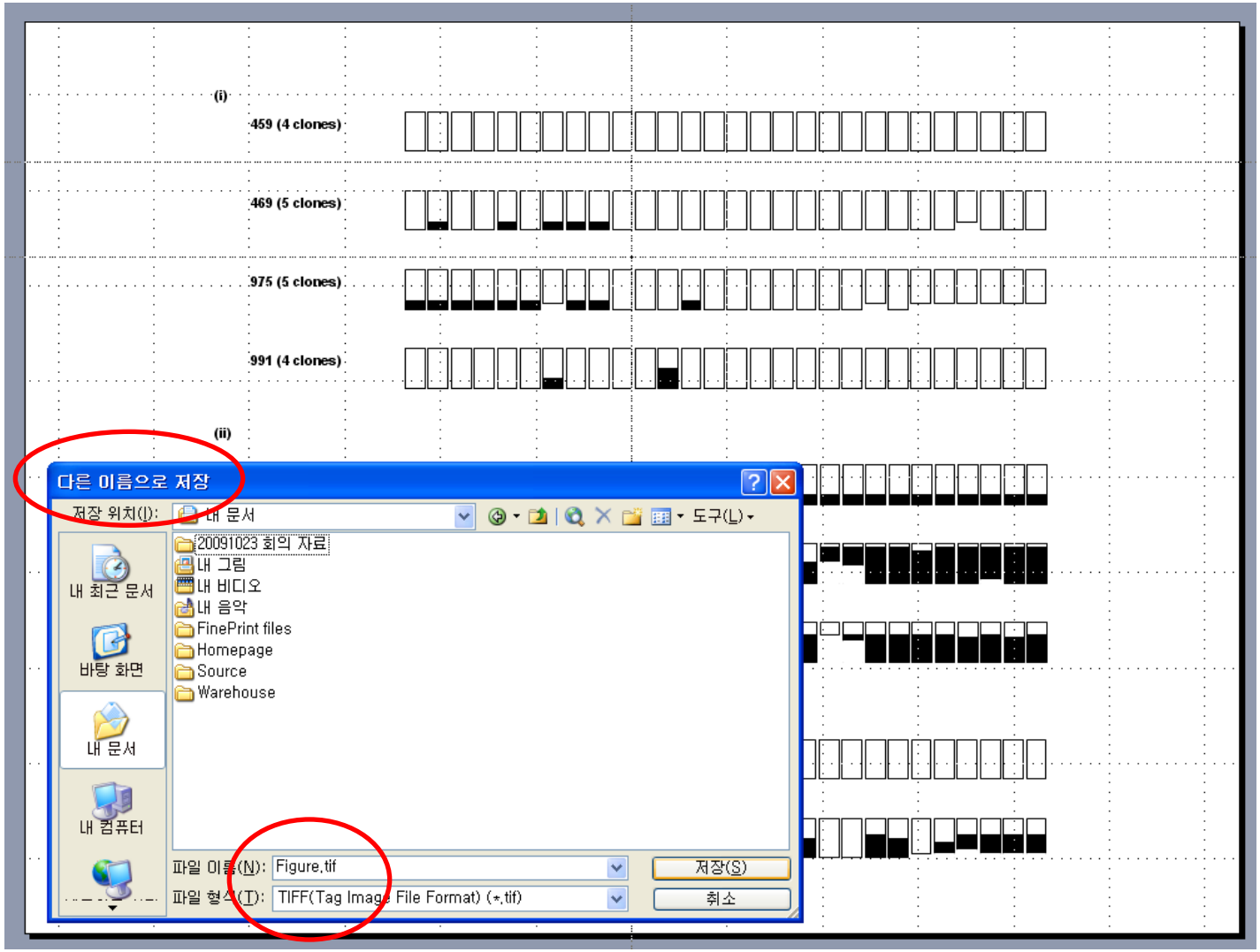

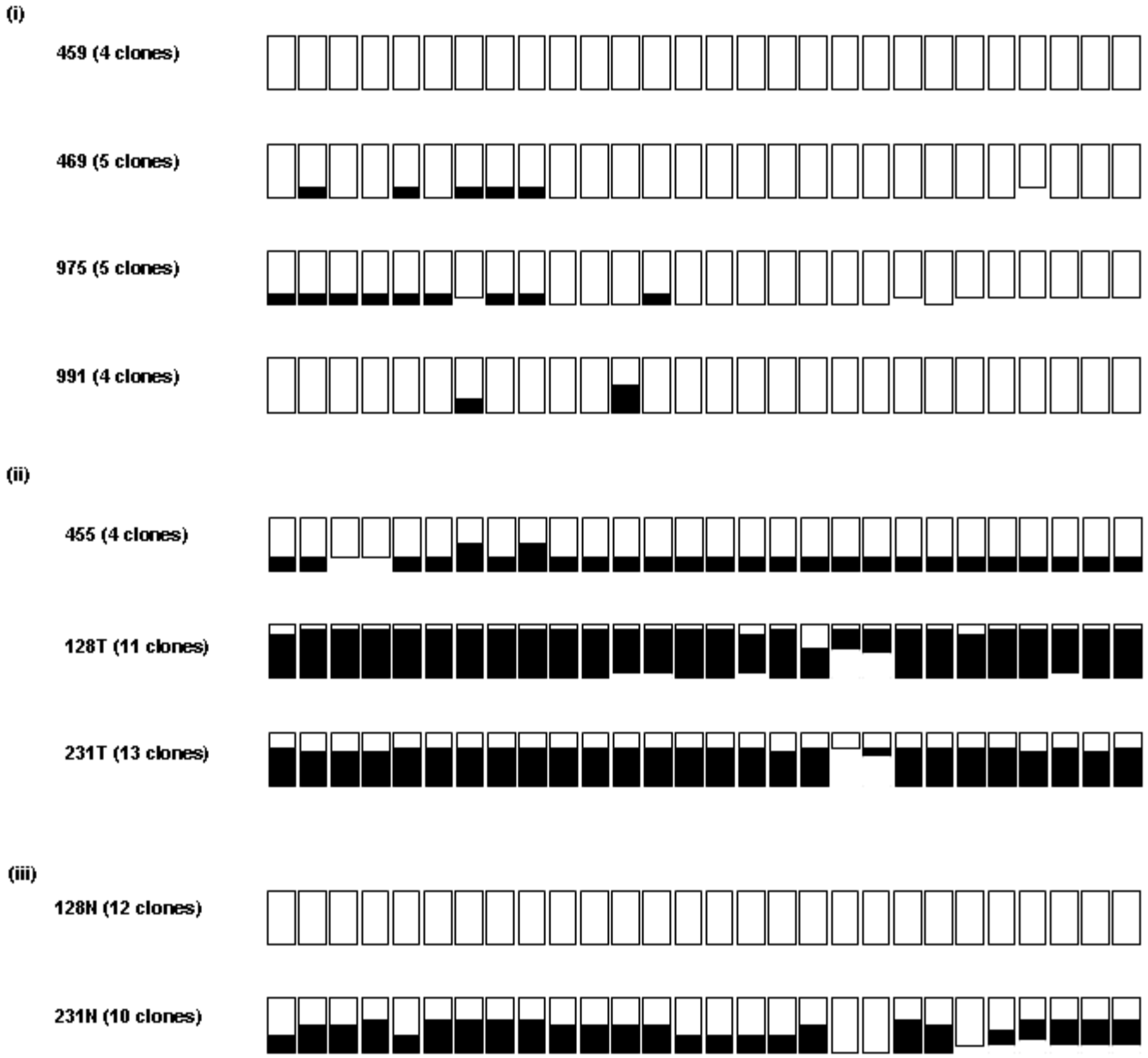
(i)
459 (4 clones)
469 (5 clones)
975 (5 clones)
991 (4 clones)
(ii)
455 (4 clones)
128T (11 clones)
231T (13 clones)
(iii)
128N (12 clones)
231N (10 clones)

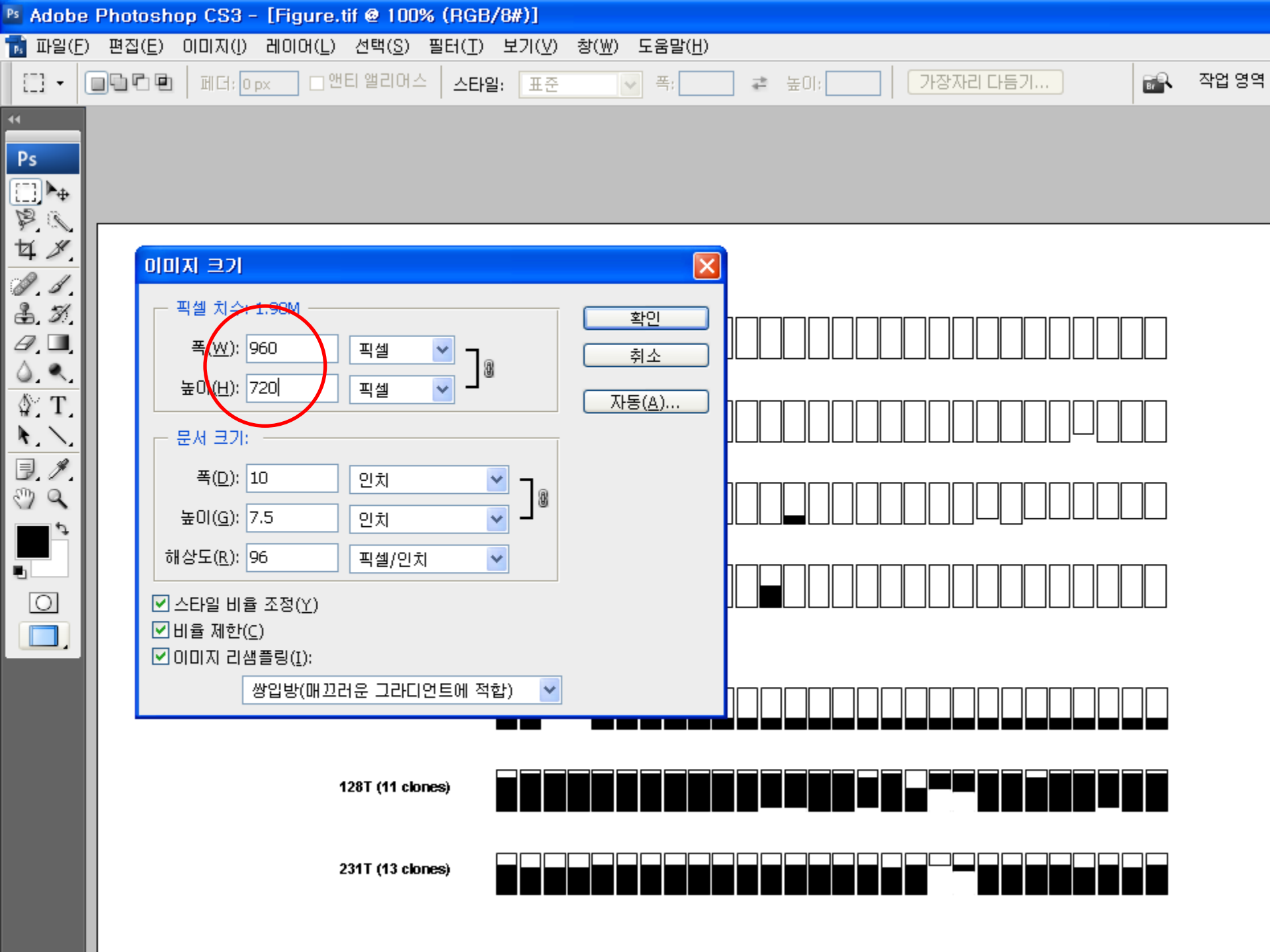
Adobe Photoshop CS3 - [Figure.tif @ 100% (RGB/8#)]
파일(F) 편집(E) 이미지(I) 레이어(L) 선택(S) 필터(T) 보기(V) 창(W) 도움말(H)
이미지 크기
픽셀 치수: 1.98M
폭(W): 960 픽셀
높이(H): 720 픽셀
문서 크기:
폭(D): 10 인치
높이(G): 7.5 인치
해상도(R): 96 픽셀/인치
스타일 비율 조정(Y)
비율 제한(C)
이미지 리샘플링(I):
쌍입방(매끄러운 그라디언트에 적합)
확인
취소
자동(A)...
128T (11 clones)
231T (13 clones)

PowerPoint 이미지를 고해상도 TIFF 파일로 바꾸는 방법

- Adobe Illustrator를 사용하는 방법
- Adobe Acrobat (혹은 Photoshop)를 사용하는 방법

Acrobat를 이용하여 PDF 파일로 변환

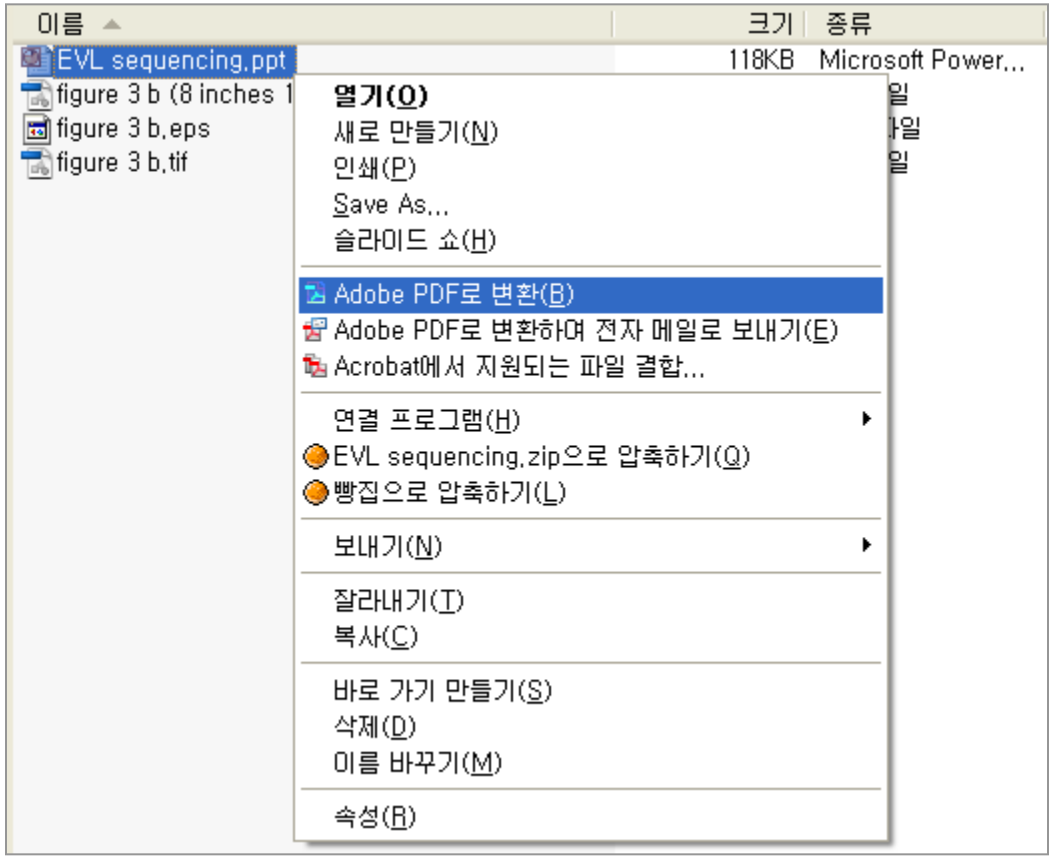

PDF 파일을 Photoshop으로 불러온다

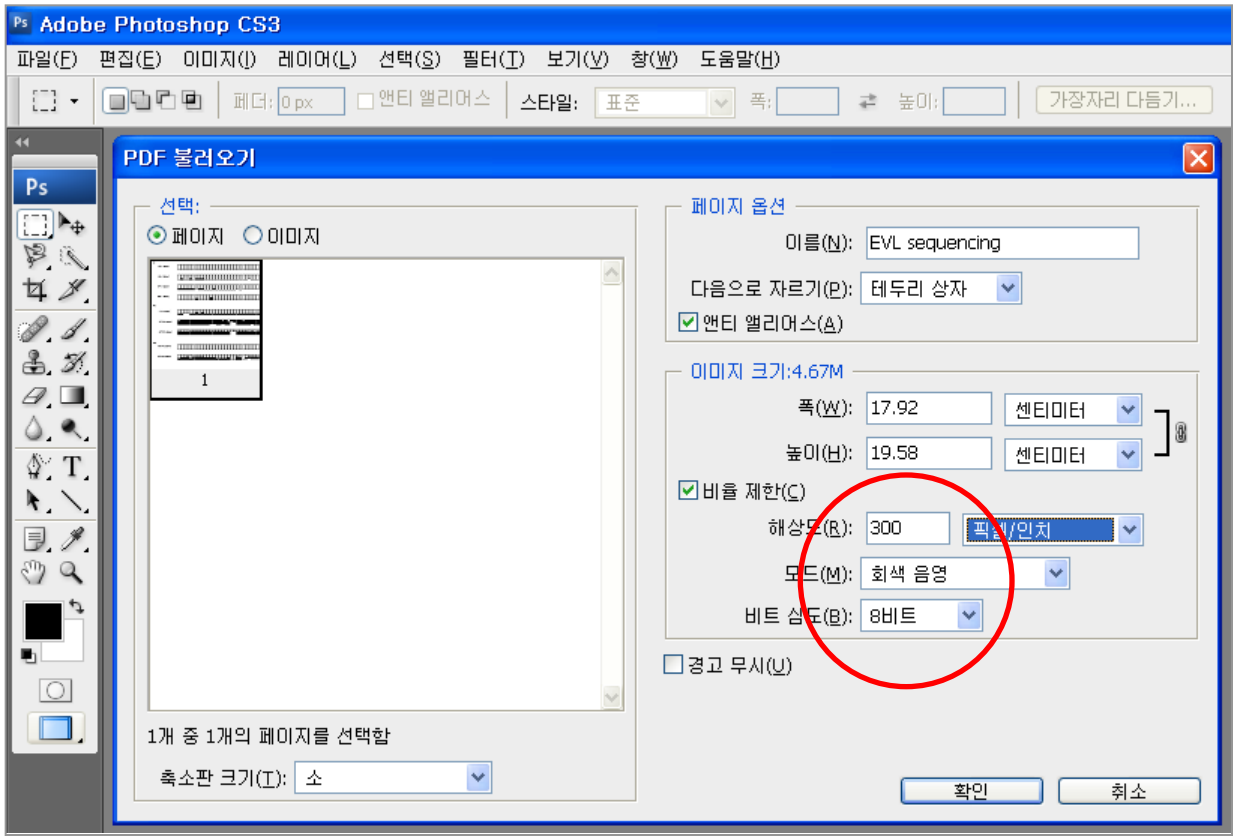

Photoshop에서 TIFF 파일로 저장한다

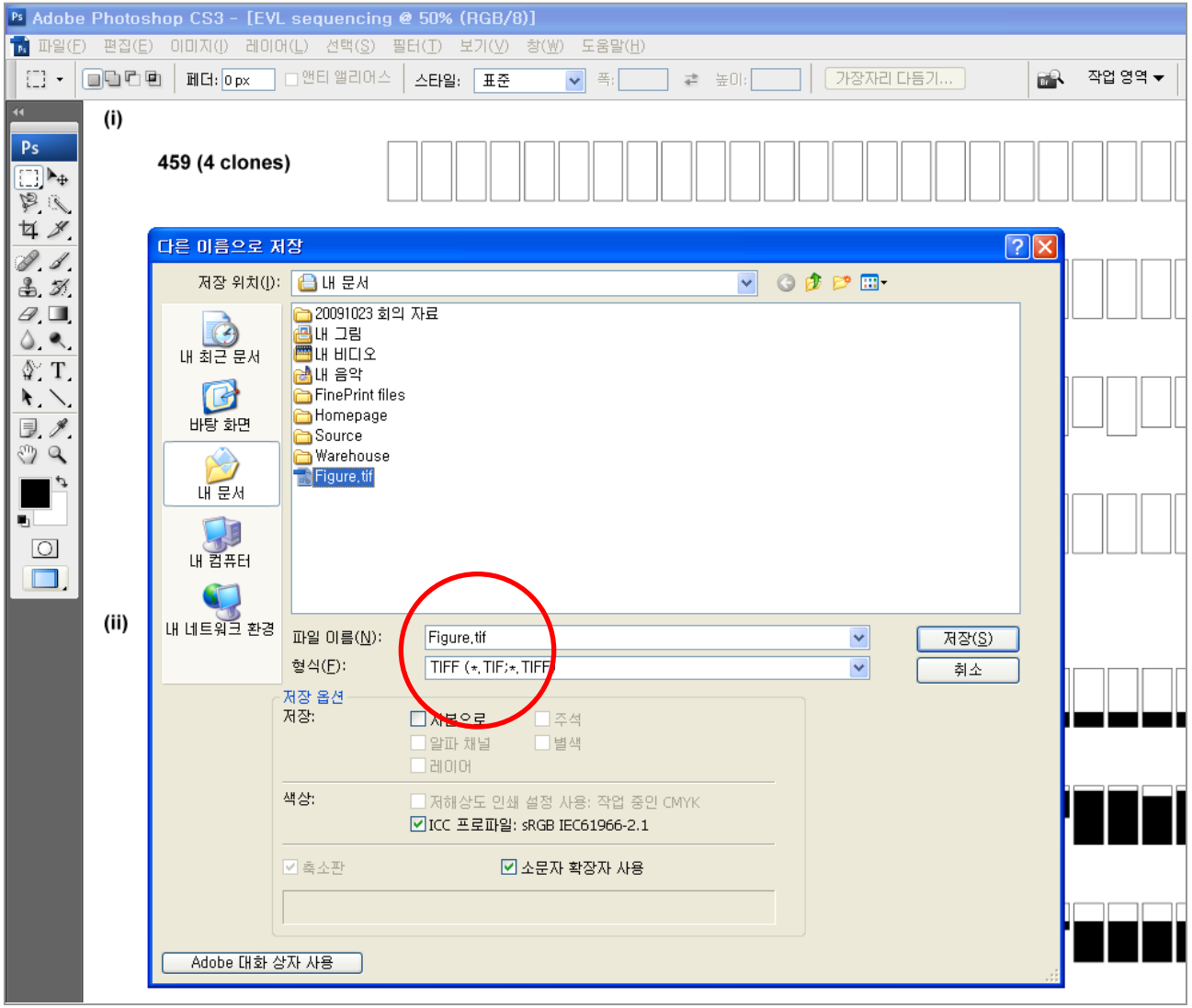

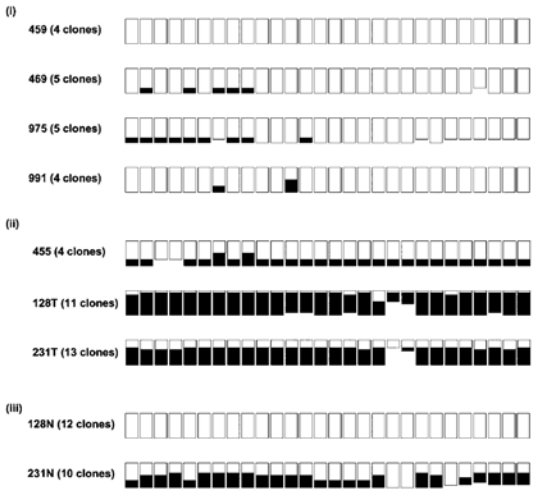

Figure 3 *EVL/hsa-miR-342* locus CpG methylation in colorectal carcinogenesis: evidence for a 'field defect' of *EVL/hsa-miR-342* locus CpG methylation in colorectal cancer. Bisulfite genomic sequencing results are shown for the *EVL/hsa-miR-342* CpG island from (i) normal colorectal mucosa from four individuals without cancer, (ii) colorectal cancer tissue from three individuals and (iii) normal appearing colorectal mucosa from two patients with concurrent colorectal cancer. The numbers in the left column represent patient identifiers. The number of clones sequenced from each patient sample is indicated in parentheses. Matched tumor (T) and normal (N) colorectal mucosa were analysed from patients no. 128 and no. 231 with results shown in (ii) and (iii). Each bar represents one CpG dinucleotide and the proportion of methylated CpGs is indicated by black shading. The height of the bar is representative of the number of informative clones at a given CpG site.

identify genes that are (a) overexpressed in colorectal cancer based on results from three relevant gene expression profiling studies (Alon *et al*., 1999; Notterman *et al*., 2001; Zou *et al*., 2002) and (b) PicTar-predicted targets of *hsa-miR-342*. Eleven genes satisfied these criteria and are presented in Supplementary Table S3.

Discussion

In this study, we confirmed that silencing of *hsa-miR-342* is a common event in colorectal cancer and provided evidence for coordinate epigenetic silencing of an intronic microRNA and its host gene in human cancer. Given that roughly half of microRNA genes are located in introns (Rodriguez *et al*., 2004; Kim and Kim, 2007; Saini *et al*., 2007), we suggest that this mode of coordinate silencing may represent a more general mechanism of microRNA suppression in human cancer.

Our data also suggest that methylation of the *EVL/hsa-miR-342* locus is an early event in colorectal carcinogenesis, given that it is detectable in 67% of adenomas, as well as in 56% of histologically normal colorectal mucosal specimens from patients with concurrent colorectal cancer. Based on these observations, we propose that the methylated DNA corresponding to the *EVL/hsa-miR-342* locus may merit further investigation as a biomarker for non-invasive disease detection or risk prediction for colorectal cancer, especially in light of its apparent specificity for colorectal cancer.

With respect to carcinogenesis, the data suggest a model in which the aberrant methylation of *EVL/hsa-miR-342* precedes histologically apparent neoplastic alterations in the colon and leads to an early expansion of precancerous progenitor cells carrying methylated CpG islands at the *EVL/hsa-miR-342* locus. The presence of methylation of *EVL/hsa-miR-342* in normal appearing colorectal mucosa may reflect an acquired, early epigenetic change in the pathogenesis of colorectal cancer. Alternatively, it could also be the consequence of clonal expansion of rare, normal colorectal epithelial cells that carry a methylated *EVL/hsa-miR-342* locus as a part of their normal physiological state (Ohm and Baylin, 2007; Widschwendter *et al*., 2007).

Given that *EVL* and *hsa-miR-342* are coordinately silenced, we cannot determine *a priori* whether suppression of *EVL*, *hsa-miR-342* or both is the relevant event in colorectal carcinogenesis. EVL is a member of the Ena/VASP protein family, which are actin-associated proteins involved in a variety of processes related to

PowerPoint 파일 → 고해상도 TIFF 요약

- PowerPoint file (vector image)를 직접 TIFF로 변환하면 960x720 px의 저해상도 TIFF로 바뀐다.
- PDF 파일(vector image)로 변환한다.
- Photoshop을 이용하여 PDF 파일을 고해상도 rastor 이미지로 불러온다.
- TIFF 형식으로 저장한다.

Take home message

- 모든 이미지는 필요에 따라 적절한 해상도로 만들어져야 한다.
- 이미지를 변경시킬 경우 원본 파일을 확실하게 back up 해 두어야 한다.
- 가능하면 그래프는 vector 형식을 이용하는 것이 좋다.
- 출판용 이미지는 고해상도가 필요하지만 PowerPoint 발표에서는 적절한 저해상도가 좋다.

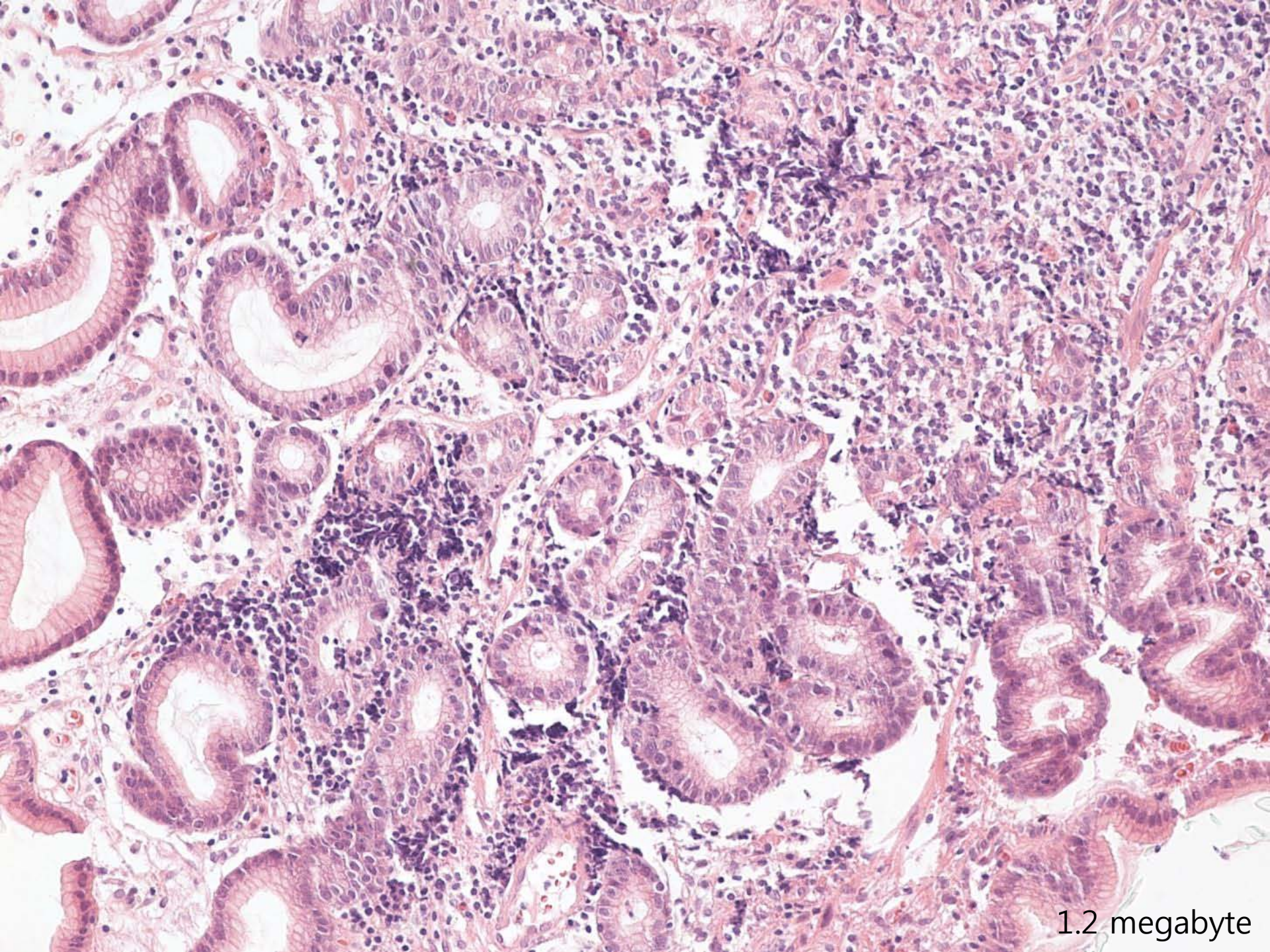
1.2 megabyte

경청해 주셔서 감사합니다.